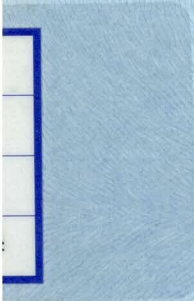


DETECTION OF CERENKOV RADIATION
EXCITED BY
A LOW-INTENSITY ELECTRON BEAM
IN
MAGNETOPLASMA

MASAYUKI FUKAO

OCTOBER 1974

Department of Nuclear Engineering
Kyoto University, Kyoto, Japan



DETECTION OF CERENKOV RADIATION
EXCITED BY
A LOW-INTENSITY ELECTRON BEAM
IN
MAGNETOPLASMA

MASAYUKI FUKAO

OCTOBER 1974

Department of Nuclear Engineering
Kyoto University, Kyoto, Japan

DOC
1974
27
電気系

ABSTRACT

RF-emission has been detected in low intensity electron beam experiments in magnetoplasma and identified with the Cerenkov radiation since its behaviour is in good agreement with the theory of the Cerenkov mode.

In order to facilitate the experiments and to avoid undesirable perturbations, a stable low pressure ECRH type plasma source, a tenuous electron beam of energies from 5 to 30 keV and a lock-in instrument of high sensitivity for RF-field measurement were used.

The spectrum and polarization of the radiation, as well as the dependence of its intensity upon the plasma and beam parameters, have been investigated. From the observed relation between the radiation intensity and the beam current, it is concluded that the radiation tends to become coherent above a certain threshold value of the beam current. The threshold value and its dependence upon beam energy were in good agreement with the stability criterion for a thin beam-plasma interaction.

CONTENTS

Abstract	i
§1 Introduction	1
§2 Theory	8
§3 Experimental Apparatus and Radiation Detection System	22
§4 Experimental Results	30
§5 Comparison of Experimental Results with Theory	42
§6 Discussion	46
§7 Conclusions	51
Acknowledgement	54
References	55
Appendix A; Cerenkov Radiation in an Isotropic Medium	56
Appendix B; Derivation of Dielectric Tensor of Cold Electron Plasma	59

§1 INTRODUCTION

Cerenkov radiation is known to be one of the great variety of dissipation processes through which charged particles in a magnetoplasma lose their kinetic energy. Elementary radiative processes such as bremsstrahlung, cyclotron- and Cerenkov-radiation have been reviewed by Bekefi¹⁾ on the basis of a good deal of experimental and theoretical materials published. The purpose of the present study is to detect and experimentally identify the Cerenkov radiation by injecting an electron beam of relatively low intensity into a magnetoplasma, and to investigate some of associate phenomena such as the coherence of radiation due to individual electrons.

At present, the Cerenkov radiation in an isotropic transparent material is a well-known phenomenon. We can easily observe the Cerenkov light in a research fission reactor of swimming-pool type and the Cerenkov effect has been applied to a Cerenkov detector which is used widely in the field of high energy physics and cosmic ray research. Historically, it is the first observation of the Cerenkov light that Marie Curie found bottles of concentrated radium solutions aglow with uncanny pale blue light in 1910. Her preoccupation with the much more significant discoveries in radioactivity stifled an investigation of the cause and nature of this luminescence. The first deliberate attempt to study the phenomenon was made by Mallet in 1926 - 1929. He found that the light

was emitted from a wide variety of transparent bodies placed close to a radioactive source with the same bluish-white quality. His studies were limited to experimental observations of the phenomenon and no attempt were undertaken to offer the explanation for the origin of the light.

Cerenkov performed an exhaustive series of experiments in 1934 - 1938. These experiments were remarkable for the excellent agreement between their results and the theory which had been proposed by Tamm and Frank in 1937²⁾.

Then the theoretical basis of the Cerenkov radiation has been confirmed. A review of experiments and theories on the Cerenkov radiation and its applications to Cerenkov counters was summerized by Jelly³⁾.

The condition that radiation is emitted by the Cerenkov effect in an isotropic dielectric medium is given by

$$\cos \theta_0 = \frac{c}{n(\omega)v}, \quad (1)$$

where θ_0 is the angle formed by the particle velocity \vec{v} and the Cerenkov wave vector \vec{k} , and $n(\omega)$ is the index of refraction at the frequency being considered ω . This condition requires that the velocity of the emitter exceeds the phase velocity of wave in the medium c/n . The radiation condition can be extended to apply in an anisotropic dielectric medium such as a crystal and a magnetoplasma, by replacing $n(\omega)$ with the refractive index in the direction of wave propagation $n(\omega, \theta_0)$ ⁴⁾. A magnetoplasma has several regions of anomalous dispersion where the cyclotron- and

hybrid-resonances take place. In the neighbourhood of each resonance frequency, the refractive index becomes very large. Consequently, the Cerenkov condition can be satisfied in a wide range of the emitter speed extending to the kilo-electron-volt region. This differs very markedly from Cerenkov emission in common transparent materials where the emitter has usually a relativistic velocity.

A theoretical study of the Cerenkov radiation in a magneto-plasma was first presented by Kolomenski⁵⁾. Since then, a number of theoretical treatments and calculation have been reported. Kurdyumov⁶⁾ ⁷⁾ investigated the condition for radiation, the spectrum and the radiation intensity in the cold plasma approximation. Sasiela and Freidberg⁸⁾ suggested the application of a C.M.A. diagram and made the radiation condition very clear. Kikuchi⁹⁾ has described a treatment which takes account of the thermal motion of background plasma particles and showed the existence of a new "plasma-mode" besides the ordinary- and extraordinary-modes.

Few reports, however, have been presented on the experimental study of the Cerenkov radiation, though there have been many studies of beam-plasma interaction. Eastlund¹⁰⁾ summarized the experimental results in Astron and other intense relativistic electron beam experiments which he compared with his theory. In these experiments, an intense pulsed relativistic electron beam was injected into a neutral gas at the relatively high pressure of 0.1 -

0.01 torr.

The elementary dissipation processes in a magneto-plasma are all weak phenomena and the radiation caused by a single test particle is extremely faint. Most of the difficulties in experimental studies of the Cerenkov effect arise from this fact. In addition, since a magnetoplasma is a highly dispersive medium, several collective phenomena other than of the Cerenkov mode may be excited at the same time, resulting an unfavorably high background radiation. Therefore, it is necessary to choose a favorable condition in which those collective modes are suppressed. The characteristic parameters of the plasma and of the injected emitters should be changed over a wide range so that the Cerenkov radiation can be identified by its dependence upon these parameters. As a matter of course, when there are N emitters passing together through a plasma with a same velocity, the intensity of total radiation is N times the single-particle-radiation, if the radiation is incoherent; if perfectly coherent, the intensity becomes N^2 times the individual radiation.

Recently, Y.Mizumachi, K.Nishikawa and T.Nishikawa reported that they observed a coherent Cerenkov radiation from a magnetized mercury plasma¹¹⁾. A highly relativistic bunched electron beam from a linear accelerator was injected into the plasma in the direction parallel to a weak magnetic field. A strong polarized radiation was observed in the propagation direction perpendicular to the axis of magnetic field, when the upper hybrid resonance

frequency was matched to the accelerator frequency (bunching frequency) which was used as the receiving frequency at the same time. It was concluded that the major properties of the observed radiation were consistently explained by assuming the coherent Cerenkov radiation of the extraordinary waves. All the experimental conditions were chosen so that the radiation became coherent and its intensity was strong enough for detection.

An experiment with a bunched beam is considered to be disadvantageous by the following reasons:

- (1) The range over which the plasma parameters can be changed is limited.
- (2) The perturbation caused by beam injection is appreciable, and so it is rather difficult to distinguish the Cerenkov radiation from the other collective phenomena.
- (3) It is impossible to study the transition from the incoherent radiation to the coherent.

It should be pointed out that even an incoherent radiation can be detected, if all the experimental conditions are carefully chosen so that the background radiation is reduced as far as possible. The intensity of the Cerenkov radiation will be rather increased than decreased when the speed of injected electron is lowered. For the purpose of obtaining a stronger radiation, therefore, the current intensity of the beam should be raised, instead of increasing the speed. With a lower speed of electron, the beam is, however, easier to suffer a density modulation and, as a result, collective phenomena due to so-called beam-plasma

interaction are apt to occur. Since those collective phenomena depend primarily upon the beam plasma frequency, i.e. the beam particle density, the dependence of observed radiation intensity and spectrum upon the beam intensity and the beam energy should carefully be examined.

This report describes a systematic experimental study about the Cerenkov radiation in magnetoplasmas.

In order to perform the experiments over a wide range of plasma parameters, an external plasma source was used.

To avoid undesirable perturbations upon the initial distribution of background plasma due to beam injection, the neutral gas pressure was made as low as possible and the beam intensity reduced to the limit of detectability of the RF-field. An ECRH plasma source was successfully

used to provide a stable discharge at low gas pressure of 10^{-4} torr or less. A lock-in method was employed to

assure high sensitivity of the radiation detection system.

Not only the frequency spectrum and polarization of the radiated wave but also the dependence of the radiation intensity upon plasma and beam parameters were investigated.

In Section 2, a theoretical treatment of Cerenkov radiation and some computational results of the spectrum and polarization are described. Section 3 describes the experimental arrangement and the measurement system, and the experimental results are given in Section 4.

In Section 5, the experimental results are compared with theory. In Section 6, we examine the perturbation caused by the beam on the background plasma and discuss the

coherence of the radiation and its relation to the beam-plasma interaction. Conclusions are listed up in Section

7. A simplified theory of the Cerenkov radiation in an isotropic medium and derivation of the dielectric tensor of a magnetoplasma in the cold plasma approximation are presented in Appendices A and B.

We consider a cold plasma in an external magnetic field \vec{B} along the z-axis. We neglect ion motion and collisions. A charge q moves along the z-axis with a constant velocity $\vec{v}_0 = \vec{\beta}c$. Then, the current density is given by

$$\vec{J} = q\vec{v}_0\delta(\vec{r} - \vec{v}_0t). \quad (2)$$

Substituting this into Maxwell's equations, we obtain for the Fourier components of electric fields having plane-wave dependence $\exp[i(\vec{k}\cdot\vec{r} - \omega t)]$,

$$(\mathbf{k}^2 - \vec{k}\vec{k} \cdot \vec{k})\vec{E}(\vec{k}, \omega) = 2\pi i\mu_0\omega q\vec{v}_0\delta(k_z v_0 - \omega) \quad (3)$$

where μ_0 and k_0 are the permeability and wave number ω/c in vacuum respectively, and \vec{k} is the dielectric tensor of the cold electron plasma, being given by

$$\vec{k} = \begin{pmatrix} \epsilon_t & -i\gamma & 0 \\ i\gamma & \epsilon_t & 0 \\ 0 & 0 & \epsilon_0 \end{pmatrix} \quad (4)$$

whose components are given by

$$\epsilon_t = 1 - \omega_{pe}^2 / (\omega^2 - \omega_{ce}^2)$$

* A simplified theory of the Cerenkov radiation in an isotropic medium is described in Appendix A.

$$\begin{aligned}\epsilon_0 &= 1 - \omega_{pe}^2/\omega^2 \\ \gamma &= -\omega_{pe}^2\omega_{ce}/[\omega(\omega^2 - \omega_{ce}^2)]\end{aligned}\quad (5)$$

where ω_{pe} and ω_{ce} are the electron plasma frequency and the electron cyclotron frequency, respectively. Derivation of the dielectric tensor of cold electron plasma is described in Appendix B.

Expressed in cylindrical coordinates, equation (3) becomes

$$\begin{aligned}\begin{pmatrix} k^2 - k_r^2 - k_0^2 \epsilon_t & ik_0^2 \gamma & -k_r k_z \\ -ik_0^2 \gamma & k^2 - k_0^2 \epsilon_t & 0 \\ -k_r k_z & 0 & k^2 - k_z^2 - k_0^2 \epsilon_0 \end{pmatrix} \begin{pmatrix} E_r \\ E_\phi \\ E_z \end{pmatrix} \\ = 2\pi i \omega \mu_0 q v_0 \delta(k_z v_0 - \omega) \begin{pmatrix} 0 \\ 0 \\ 1 \end{pmatrix}.\end{aligned}\quad (6)$$

By inverse Fourier transformation, we obtain the following expression for the component of the electric field parallel to the charge velocity;

$$\begin{aligned}E_z(r, z, t) &= \frac{1}{(2\pi)^4} \int_{-\infty}^{\infty} d\omega \int_0^{\infty} k_r dk_r \int_0^{2\pi} d\phi \int_{-\infty}^{\infty} dk_z e^{i(k_r r \cos\phi + k_z z - \omega t)} E_z(\vec{k}, \omega) \\ &= \frac{i\mu_0 q}{(2\pi)^2} \int_{-\infty}^{\infty} \omega d\omega \int_0^{\infty} \kappa d\kappa J_0(\kappa k_0 r) \frac{(\epsilon_t - \beta^{-2})(\kappa^2 - \epsilon_t + \beta^{-2}) + \gamma^2}{D(\kappa, \omega)} \\ &\quad \times e^{-i\omega(t - z/v_0)}\end{aligned}\quad (7)$$

where $\kappa = k_r/k_0$ and

$$D(\kappa, \omega) = (\kappa^2 - \epsilon_t + \beta^{-2})(\epsilon_t \kappa^2 - \epsilon_0 \epsilon_t + \epsilon_0 \beta^{-2}) + \gamma^2(\kappa^2 - \epsilon_0). \quad (8)$$

$D(\kappa, \omega) = 0$ gives a dispersion relation under the condition that the phase velocity along the external magnetic field is equal to the velocity of the moving charge, as shown in Fig.1.

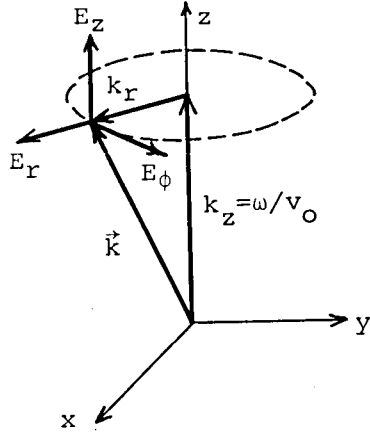


Fig.1. Wave vector and polarization of electric field.
Cerenkov condition is given by $k_z = \omega/v_0$.

The total energy W radiated per unit path length is equal to the work done by the charge per unit path length against the force $F = -qE_z$ reacting on the charge.

Therefore, we obtain

$$\begin{aligned} \frac{dW}{dz} &= -qE_z(\vec{r} = \vec{v}_0 t) \\ &= -\frac{i\mu_0 q^2}{(2\pi)^2} \int_{-\infty}^{\infty} \omega d\omega \int_0^{\infty} \kappa d\kappa \frac{(\epsilon_t - \beta^{-2})(\kappa^2 - \epsilon_t + \beta^{-2}) + \gamma^2}{D(\kappa, \omega)} \end{aligned} \quad (9)$$

where the electric field is taken at the location of the charge $r = 0$ and $z = v_0 t$. Since $D(\kappa, \omega)$ is an even function of ω , it is obvious that the principal part of the

integral with respect to ω vanishes. The radiation intensity is determined by the singular part of the ω -integral. When there is no positive root of κ which satisfies $D(\kappa, \omega) = 0$, it is easily shown that there occurs no radiation. In order to calculate the singular part, we must carefully determine the integration path in the neighbourhood of the positive pole. Introducing an infinitesimal dissipation through collisions of the electrons with ions and/or neutral atoms, the elements of the dielectric tensor are modified as derived in Appendix B;

$$\begin{aligned} \epsilon_t &\rightarrow \epsilon_t + i\nu\epsilon'_t & \text{with } \epsilon'_t &= \frac{\omega_{pe}^2(\omega^2 + \omega_{ce}^2)}{\omega(\omega^2 - \omega_{ce}^2)^2} \\ \epsilon_0 &\rightarrow \epsilon_0 + i\nu\epsilon'_0 & \text{with } \epsilon'_0 &= \frac{\omega_{pe}^2}{\omega^3} \\ \gamma &\rightarrow \gamma + i\nu\gamma' & \text{with } \gamma' &= \frac{2\omega_{pe}^2\omega_{ce}}{(\omega^2 - \omega_{ce}^2)^2} \end{aligned} \quad (10)$$

where ν denotes the collision frequency, therefore is positive. It is easily seen that all the imaginary parts are positive for $\omega > 0$. Using these expressions in $D(\kappa, \omega)$, we obtain*

$$D(\kappa, \omega) = \epsilon_t [\kappa^2 - (\kappa_+^2 + i\Omega_+)] [\kappa^2 - (\kappa_-^2 + i\Omega_-)] \quad (11)$$

$$\text{where } \kappa_{\pm} = B \pm \sqrt{B^2 - C} \quad (12)$$

$$\begin{aligned} \text{with } B &= [(\epsilon_t - \beta^{-2})(\epsilon_t + \epsilon_0) - \gamma^2] / 2\epsilon_t \\ C &= \epsilon_0 [(\epsilon_t - \beta^{-2})^2 - \gamma^2] / \epsilon_t \end{aligned} \quad (13)$$

$$B^2 - C = \{[(\epsilon_t - \beta^{-2})(\epsilon_t - \epsilon_0) - \gamma^2]^2 + 4\gamma^2\epsilon_0\beta^{-2}\} / 4\epsilon_t^2.$$

* To have positive root of κ , $B^2 - C$ must be positive.

The imaginary parts of the κ^2 s which satisfy $D(\kappa, \omega) = 0$ are given by

$$\Omega_{\pm} = \pm \frac{\nu}{\sqrt{B^2 - C}} (\kappa_{\pm}^2 B' - C'/2) \quad (14)$$

where

$$B' = \frac{1}{2\varepsilon_t^2} (\varepsilon_t^2 + \varepsilon_0 \beta^{-2} + \gamma^2) \varepsilon_t' + \frac{1}{2\varepsilon_t} (\varepsilon_t - \beta^{-2}) \varepsilon_0' - \frac{\gamma}{\varepsilon_t} \gamma' \quad (15)$$

$$C' = \frac{\varepsilon_0}{\varepsilon_t^2} (\varepsilon_t^2 - \beta^{-4} + \gamma^2) \varepsilon_t' + \frac{1}{\varepsilon_t} [(\varepsilon_t - \beta^{-2})^2 - \gamma^2] \varepsilon_0' - \frac{2\varepsilon_0 \gamma}{\varepsilon_t} \gamma'.$$

Substituting all the above expressions into equation (9), expanding the integrand into partial fractions, we obtain

$$\frac{dW}{dz} = - \frac{i\mu_0 q^2}{16\pi^2} \int_{-\infty}^{\infty} \left(1 - \frac{1}{\varepsilon_t \beta^2}\right) \omega d\omega \int_0^{\infty} dk^2 \left[\frac{1 - \psi}{\kappa^2 - (\kappa_+^2 + i\Omega_+)} + \frac{1 + \psi}{\kappa^2 - (\kappa_-^2 + i\Omega_-)} \right] \quad (16)$$

where

$$\psi = \frac{\varepsilon_t (\varepsilon_t - \beta^{-2})(\varepsilon_t - \varepsilon_0) - \gamma^2 (\varepsilon_t + \beta^{-2}) / (\varepsilon_t - \beta^{-2})}{|\varepsilon_t| \sqrt{[(\varepsilon_t - \beta^{-2})(\varepsilon_t - \varepsilon_0) - \gamma^2]^2 + 4\gamma^2 \varepsilon_0 \beta^{-2}}} \quad (17)$$

If neither κ_+^2 nor κ_-^2 is positive, the integral with respect to ω in equation (16) vanishes when $\nu \rightarrow 0$, because ε_t , ε_0 and γ^2 are even functions of real ω . Since κ_{\pm}^2 and Ω_{\pm} are even and odd functions of the frequency variable ω , respectively, the integration with respect to ω in equation (16) can be rewritten in the form

$$\int_{-\infty}^{\infty} \omega d\omega f(\omega) \int_0^{\infty} dk^2 \frac{1}{\kappa^2 - (\kappa_{\pm}^2 + i\Omega_{\pm})}$$

$$= \int_0^{\infty} \omega d\omega f(\omega) \int_0^{\infty} dk^2 \left[\frac{1}{\kappa^2 - (\kappa_{\pm}^2 + i\Omega_{\pm})} - \frac{1}{\kappa^2 - (\kappa_{\pm}^2 - i\Omega_{\pm})} \right] \quad (18)$$

where $f(\omega)$ is an even function of real ω .

When ν approaches to zero, the poles $\kappa_{\pm}^2 + i\Omega_{\pm}$ and $\kappa_{\pm}^2 - i\Omega_{\pm}$ move in the κ^2 -plane onto the real axis from above or below depending upon the sign of their respective imaginary parts. Then if either κ_{+}^2 or κ_{-}^2 is positive, the integration path with respect to κ^2 should, by analytical continuation, go around about the real positive pole; it should pass under or over such a pole if the imaginary part is positive or negative, respectively. Thus, it can easily be shown that the principal part of the κ^2 -integral in the expression (18) vanishes and only the contour integral around the poles remain. Each of the contour is clockwise or counterclockwise when Ω_{\pm} is positive or negative, respectively. Consequently, in the limit $\nu \rightarrow 0$, the κ^2 -integral in the expression (18) can be represented by the residue at κ_{\pm}^2 , hence equation (18) becomes

$$\begin{aligned} \lim_{\nu \rightarrow 0} \int_{-\infty}^{\infty} \omega d\omega f(\omega) \int_0^{\infty} d\kappa^2 \frac{1}{\kappa^2 - (\kappa_{\pm}^2 + i\Omega_{\pm})} \\ = 2\pi i \operatorname{sign}(\Omega_{\pm}) \int_0^{\infty} \omega d\omega f(\omega), \end{aligned} \quad (19)$$

where $\operatorname{sign}(\Omega_{\pm})$ is a sign factor with absolute value unity.

Upon substituting these expression into equation (16),

it finally follows that

$$\begin{aligned} \frac{dW}{dz} = \frac{\mu_0 q^2}{8\pi} \left[\int_{\substack{\omega > 0 \\ \kappa_{+}^2 > 0}} \left(1 - \frac{1}{\epsilon_t \beta^2}\right) (1 - \psi) \operatorname{sign}(\Omega_{+}) \omega d\omega \right. \\ \left. + \int_{\substack{\omega > 0 \\ \kappa_{-}^2 > 0}} \left(1 - \frac{1}{\epsilon_t \beta^2}\right) (1 + \psi) \operatorname{sign}(\Omega_{-}) \omega d\omega \right] \end{aligned} \quad (20)$$

This expression is the same as that has been derived by Kurdyumov⁶⁾.

By tracing back the derivation of equation (20), it can readily be shown that this expression is exactly equivalent to

$$\frac{dW}{dz} = \frac{\mu_0 q^2}{8\pi} \int_0^{\infty} \omega d\omega \sum_{\kappa > 0} \text{Res.} \left[\kappa \frac{(\epsilon_t - \beta^{-2})(\kappa^2 - \epsilon_t + \beta^{-2}) + \gamma^2}{D(\kappa, \omega)} \right] \text{sign}(\Omega) \quad (21)*$$

where the sum is taken for all singular points on the real axis of κ -plane. The sign factor $\text{sign}(\Omega)$ is positive or negative depending upon the dielectric properties of the medium and the velocity of moving charge. The integrand of equation (20) or (21) primarily determines the frequency spectrum of the radiated power. The radial refractive index n_r is equal to the positive root κ of the dispersion equation $D(\kappa, \omega) = 0$, while the axial index n_z is β^{-1} . The Cerenkov cone is determined by n_r and n_z . Therefore, when there are two singular points on the positive real axis of the κ -plane, two Cerenkov cones exist corresponding to the first and the second term of equation (20).

The frequency regions where the Cerenkov radiation occurs and their dependence upon plasma parameters and emitter velocity have been described with a C.M.A. diagram^{12) 13)} by Sasiela and Freidberg⁸⁾. An example of the diagram is shown in Fig.2. The abscissa $(\omega_{pe}/\omega)^2$ is proportional to plasma density and the ordinate $(\omega_{ce}/\omega)^2$ to the square of magnetic field intensity. In the diagram, the shaded

* For practical machine computation, equation (21) is more convenient than Kurdyumov's formula (20).

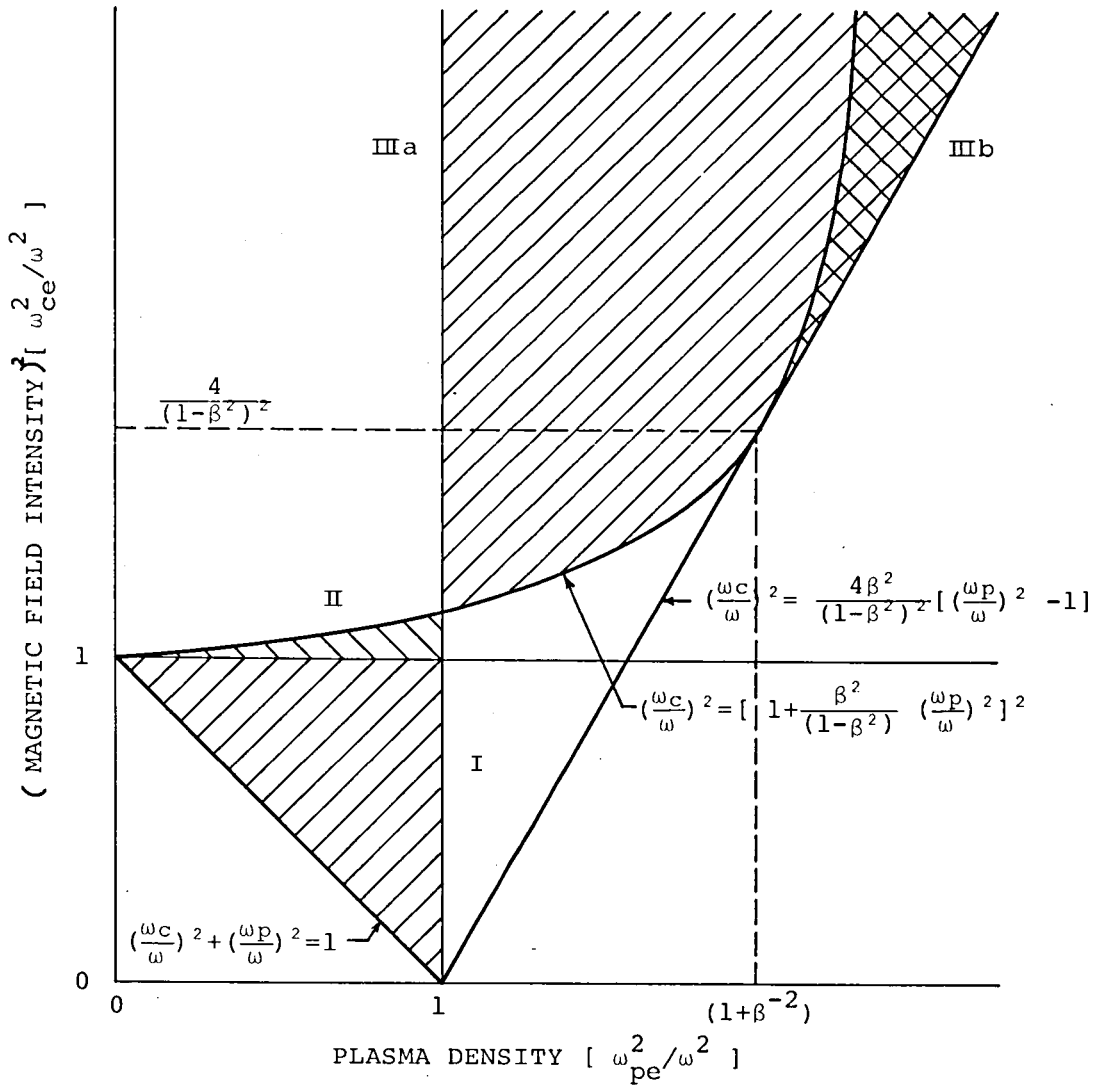


Fig. 2. Regions of the Cerenkov radiation. (from reference (8))
 Shaded regions correspond to radiation with a single cone and cross-hatched region to two cones.

regions labeled I, II and IIIa correspond to radiation with a single cone, while the cross-hatched region IIIb corresponds to two cones. The diagram shown in Fig.2 is deformed so that all the regions may be presented in a proper size easy to see. The equations defining the boundaries between adjoining regions are presented in the figure.

When a plasma density and an intensity of applied magnetic field are given, both ω_{pe} and ω_{ce} are determined. If a velocity of emitter particle, or the factor β , is also given, all the regions of the Cerenkov radiation are determined on the C.M.A. diagram as illustratively shown in Fig.2.

In order to find the frequency intervals in which emission occurs for a given magnetoplasma and an emitter speed, we have only to plot the straight line passing through the origin with the inclination $\omega_{ce}^2/\omega_{pe}^2$ and determine those frequencies for which this straight line intersects the shaded regions. It is easily seen that, in region I, radiation always occurs for any plasma and emitter parameters. A high β enlarges the area of region II and shifts the radiation spectrum of regions IIIa and IIIb to low frequencies.

Since it is the slow wave among two propagation modes in cold plasma that satisfies the Cerenkov condition, it is concluded from the C.M.A. diagram that radiated wave is the extraordinary mode in regions I and II, and the ordinary mode in regions IIIa and IIIb.

The polarization of the radiated wave is determined by equation (6) except in the neighbourhood of the charge where the radiated wave cannot be expanded into plane wave for the singularity. The components of electric fields perpendicular to the axis of external magnetic field, E_r and E_ϕ can also be obtained from equation (6) in a similar way. The results are as follows;

$$E_r(r, z, t) = \frac{i\mu_0 q}{(2\pi)^2} \int_{-\infty}^{\infty} \omega d\omega \int_0^{\infty} dk \frac{\kappa^2 \beta^{-1} (\kappa^2 - \epsilon_t + \beta^{-2})}{D(\kappa, \omega)} e^{-i\omega(t-z/v_0)}$$

$$\begin{aligned}
&= - \frac{\mu_0 q}{2\pi} \int_0^\infty \omega d\omega \sum_{\kappa > 0} \text{Res.} \left[\frac{\kappa^2 \beta^{-1} (\kappa^2 - \epsilon_t + \beta^{-2})}{D(\kappa, \omega)} e^{-i\omega(t-z/v_0)} \right] \\
&\quad \times \text{sign}(\Omega), \quad (22)
\end{aligned}$$

$$\begin{aligned}
E_\phi(r, z, t) &= - \frac{\mu_0 q}{(2\pi)^2} \int_{-\infty}^\infty \omega d\omega \int_0^\infty d\kappa \frac{\kappa^2 \gamma \beta^{-1}}{D(\kappa, \omega)} e^{-i\omega(t-z/v_0)} \\
&= - \frac{i\mu_0 q}{2\pi} \int_0^\infty \omega d\omega \sum_{\kappa > 0} \text{Res.} \left[\frac{\kappa^2 \gamma \beta^{-1}}{D(\kappa, \omega)} e^{-i\omega(t-z/v_0)} \right] \\
&\quad \times \text{sign}(\Omega). \quad (23)
\end{aligned}$$

An example of spectrum calculated for $\omega_{ce} = 0.68 \omega_{pe}$ and electron energy 20 keV ($\beta = 0.272$) is shown in Fig.3, in which the total radiated power is proportional to E_z . The field components E_r and E_ϕ , the radial refractive index n_r and the axial index n_z are also shown in Fig.3. We can notice a double cones in the low frequency region. The radiation intensity of one among the two cones is much less than that of the other. In the extraordinary mode, the radiation intensity diverges to infinity at the upper hybrid resonance frequency $\omega_{uh} = \sqrt{\omega_{pe}^2 + \omega_{ce}^2}$. This is due to the cold plasma approximation. Actually, however, the radiation intensity is limited at frequencies near ω_{uh} by the thermal motion of particles in the medium, since the phase velocity approaches the thermal velocity owing to the very large refractive index n_r at these frequencies and, in consequence, the emission is suppressed by Landau damping.

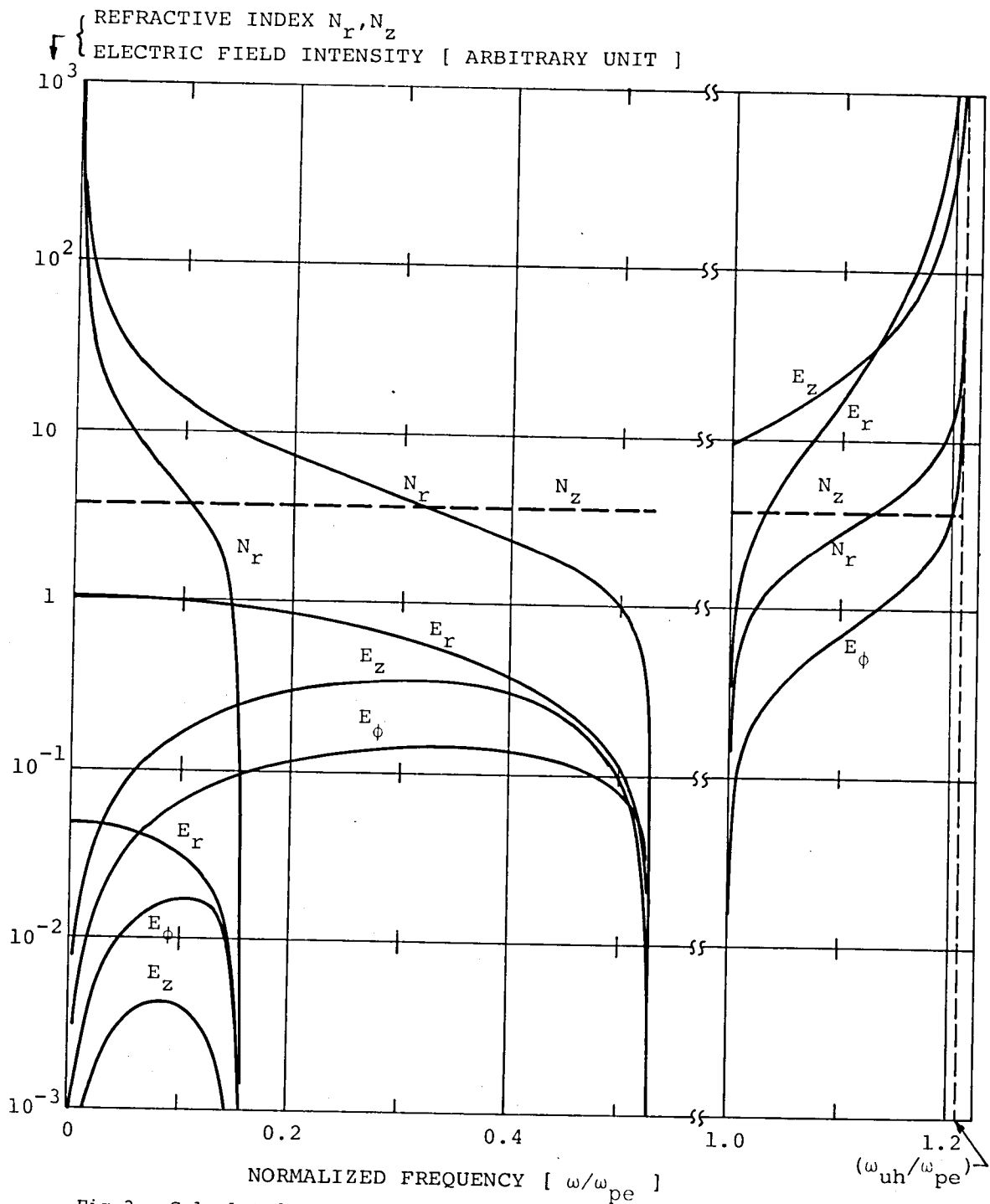


Fig.3. Calculated radiation spectrum, polarization and refractive index for the condition; $\omega_{ce} = 0.68 \omega_{pe}$, $\beta = 0.272$ (20 keV electron). Radiation intensity is proportional to E_z

The dependence of radiation intensity upon the velocity of emitter is shown in Fig.4. Radiation intensity is larger for low energy particle than for high energy in the neighbourhood of the upper hybrid resonance. This results from the fact that an emitter with a slow speed interacts with the induced electric polarization during a longer period per unit path than a fast emitter. An emitter with a high energy, however, widens the radiation spectrum in the low frequency region which corresponds to the region labeled II in Fig.2.

The above description applies to a single moving charged particle. When many charged particles stream as a beam, each one interacts with the electric field induced by the other particles as well as its own. In the case of random spatial distribution of beam particles, there is no effect from the other particles because of phase mixing of the induced electric fields. Then, the total radiation power is given by a simple summation of the individual radiations. If the beam is bunched within a space smaller than the wave length of the radiated wave in the medium, a coherence occurs and the total radiation power increases over the simple summation by a factor up to the number of the bunched particles, that is, the intensity becomes proportional to the square of the number of particles. This can be seen by replacing q in equation (9) by nq , where n is the number of bunched particles. As the number density of moving charges is increased, it becomes necessary to consider the beam particles as a part of the medium in

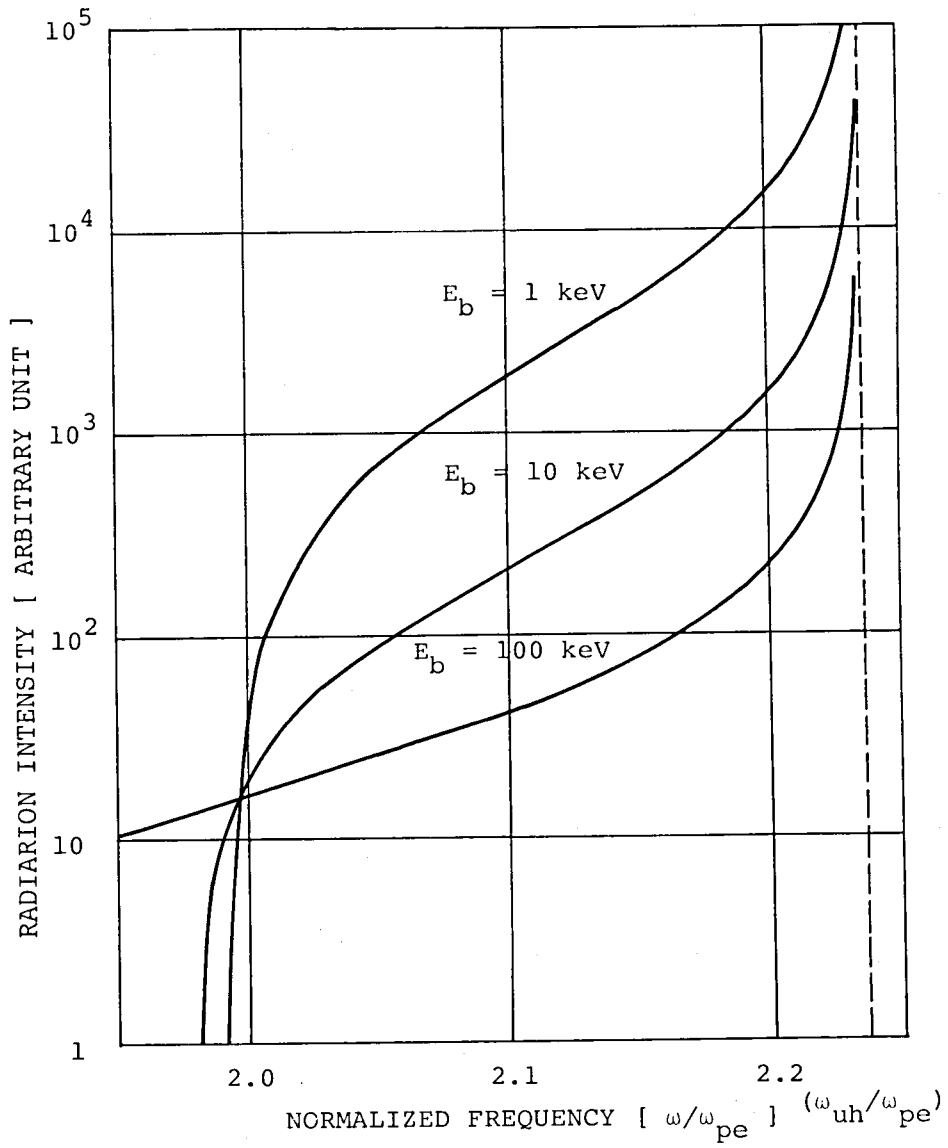


Fig.4. Calculated radiation spectra for $\omega_{ce} = 2.0 \omega_{pe}$ and electron energies $E_b = 1, 10$ and 100 keV.

calculating the electric field. In this case, the problem becomes that of a beam-plasma interaction which has been studied by many researchers (e.g. Briggs¹⁴). The treatment of beam-plasma interaction involves the kinetics of the beam particles, therefore the mass of the moving charge is important. In a beam-plasma interaction the density of beam particles is modulated by a wave propagating along the beam and a perturbation of the density causes the wave to grow. The growth rate is characterized by the beam particle density. The interaction is discussed later in connection with the coherence of radiation.

§3 EXPERIMENTAL APPARATUS AND RADIATION DETECTION SYSTEM

A schematic diagram of the experimental apparatus is shown in Fig.5. Plasma was produced by an electron cyclotron resonance heating (ECRH) discharge in a Pyrex tube of a 30 mm diameter inserted coaxially into a cylindrical cavity of an 85 mm diameter and 120 mm long. The cavity was excited by microwaves with a frequency 2450 MHz and a power up to 600 W generated by a magnetron. A circulator was employed to protect the magnetron against a standing wave with large amplitude due to wave reflection. The microwawe power was adjusted by an attenuator of reactive type. The source plasma was diffused into an interaction chamber, consisting of a Pyrex tube of an 80 mm inner diameter and 1,200 mm long, evacuated by a 4 inch oil diffusion pump system to a base pressure of 2×10^{-6} torr. The gas pressure was from 2 to 10×10^{-5} torr in an operation condition. Argon was used throughout this experiment. An electron gun was connected to the opposite end of the interaction chamber through an orifice of a 5 mm diameter and 50 mm long which formed an barrier for differential pumping. Another 2 inch oil diffusion pump maintained the gas pressure around the gun below 5×10^{-6} torr during operation.

The intensity of the applied magnetic field is also shown in Fig.5. The intensities of the mirror fields, B_0 and B'_0 , and of the uniform field B_1 which was more than 900 mm long, could be changed independently by two separate

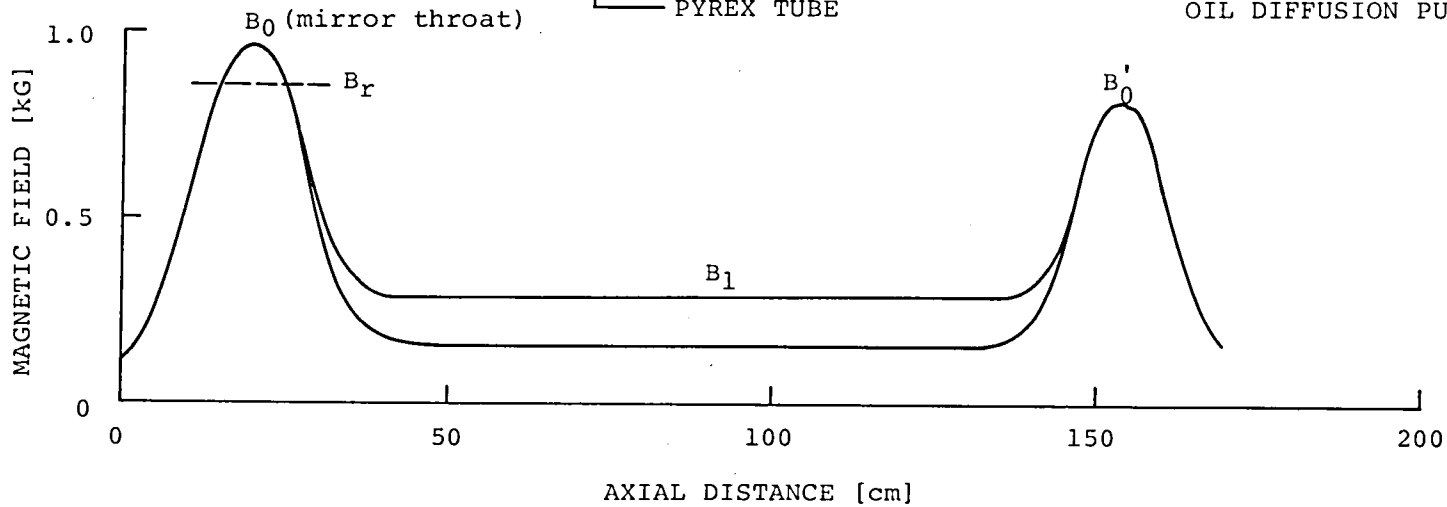
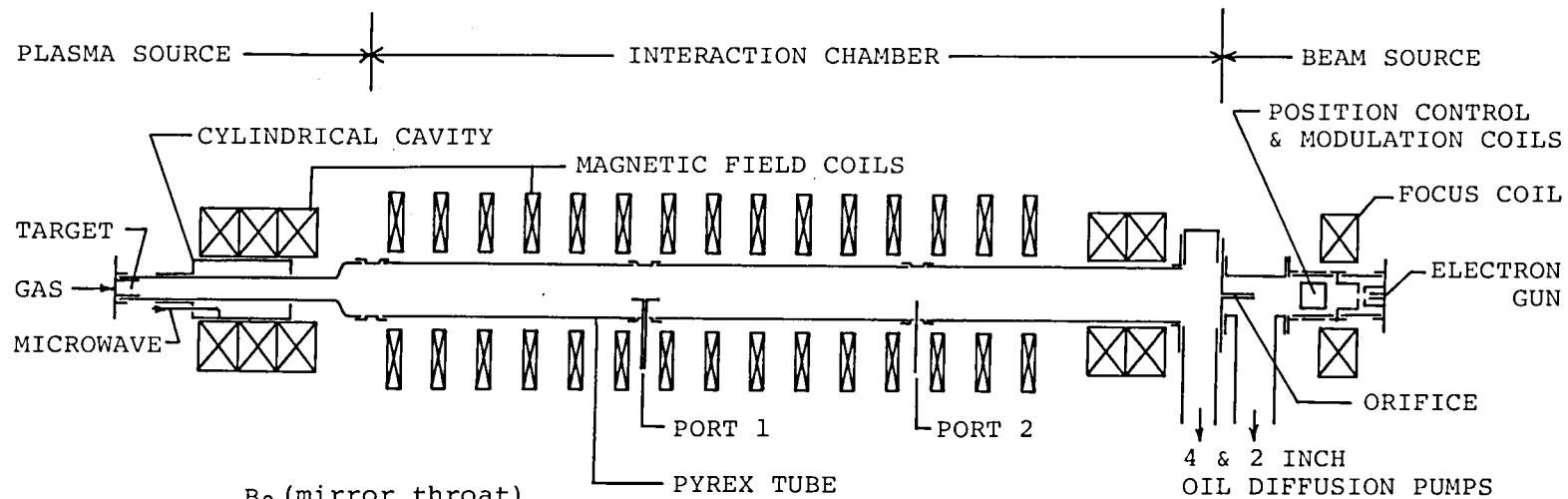


Fig.5. Schematic diagram of experimental equipment.

power supplies. The temporal ripple of the fields and the spatial ripple of the uniform field B_1 were maintained below 1 per cent

The ECRH plasma source was operated in the fundamental mode and the resonance field intensity B_{res} was equal to 875 G. The maximum field intensity B_0 at the left mirror throat was chosen to be slightly larger than the resonance intensity B_{res} , therefore, the resonant point was located in the vicinity of the throat as shown in Fig.5.

Both the resonant point and the mirror throat were inside the ECRH cavity. The ECRH discharge in a mirror field is advantageous by the following reasons:

- (1) The operation is stable at a low gas pressure.
- (2) No such steep potential gradient as in a positive column is caused in the plasma column.
- (3) There is no sputtering of impurity because of the electrode-less discharge.
- (4) Streaming of electrons and ions other than the test particles does not take place. In a positive column, such an undesirable streaming is apt to occur.

A typical example of the Langmuir probe characteristic of the plasma diffused from the ECRH cavity into the interaction chamber is shown in Fig.6. The gas pressure was 5×10^{-5} torr Argon and the uniform magnetic field $B_1 = 170$ G. Typical examples of radial distributions of the beam current and the plasma density are as shown in Fig.7. The conditions are the same as for Fig.6. The density profiles shown in Fig.7 were measured through ion saturation current of the

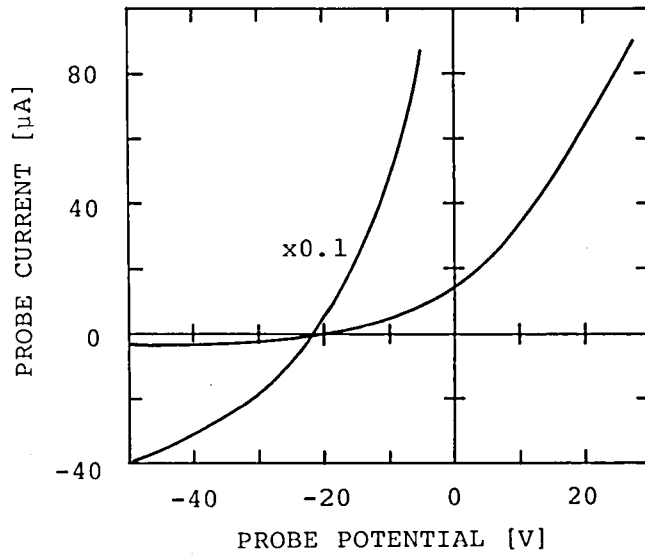


Fig.6. Typical example of the Langmuir probe characteristic of the plasma in the interaction chamber. Conditions; $p = 5 \times 10^{-5}$ torr Ar, $B_1 = 170$ G.

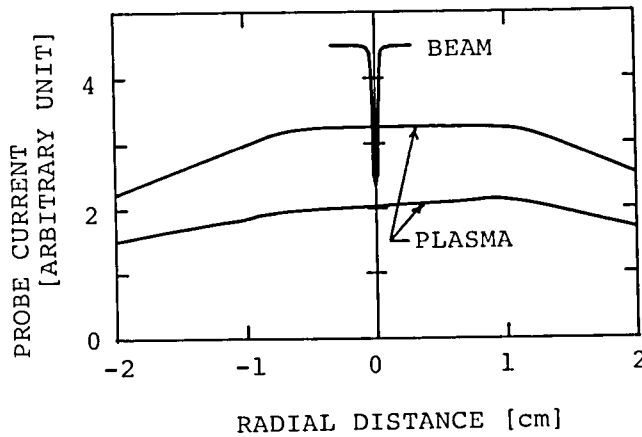


Fig.7. Typical examples of beam- and plasma-profiles. Conditions; probe potential = - 50 V and the same as Fig.6.

probe biased to -50 V. Typical parameters of the diffused plasma in the interaction chamber were $n_e = 5 \times 10^9 \text{ cm}^{-3}$, $T_e = 12.5 \text{ eV}$ and plasma diameter = 60 mm for $B_0 = 1000 \text{ G}$, $B_1 = 200 \text{ G}$, gas pressure = $5 \times 10^{-5} \text{ torr}$ and microwave power = 100 W. Changing B_1 had no appreciable influence on the operation of the ECRH plasma source discharge but had a significant effect on the density and the diameter of the diffused plasma in the interaction chamber.

The plasma density increased in proportion to B_1 or $B_1^{1.5}$. It was not possible to obtain a sufficient variation in plasma density by merely adjusting the microwave power at a fixed field strength B_1 . In order to vary the plasma density over a wider range the magnetic field B_0 in the source region and the axial position of the cylindrical cavity were adjusted together. These adjustments had no appreciable effect on the electron temperature and density profile, provided the ECRH resonant region was located within the cavity.

The control circuit of the electron beam and the radiation detection system are shown in Fig.8. The electron gun used is a simple one consisting of a filament of thoriated tungsten wire, a Wehnelt electrode and an extraction electrode. The filament is made of thoriated tungsten wire of a 0.23 mm diameter wound to form a cylinder, 1.5 mm in diameter and 1.5 mm long. A floating battery was used to heat the filament. The beam was focused magnetically and two pairs of auxiliary coils were used to control the beam position. The diameter of the beam was 2 mm or less in the interaction chamber.

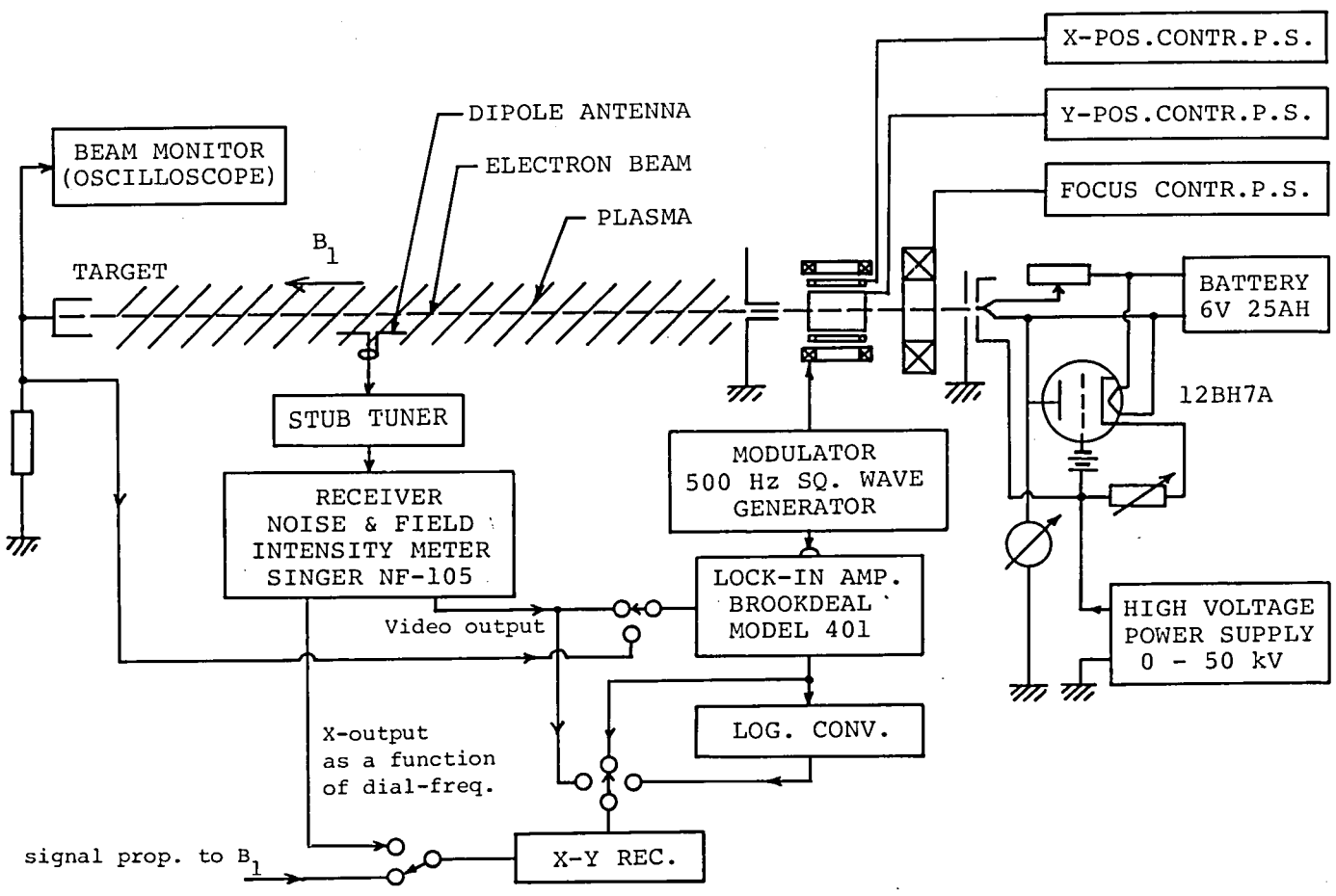


Fig.8. Schematic diagram of electron beam controller and radiation detection system.

The collector was a Faraday cylinder made of aluminum to avoid unnecessary X-ray radiation. A simple X-ray shield of lead sheets was also used. The electron beam could be varied from 5 to 30 keV in energy and from 0.1 to 2.5 mA in current. The beam current was stabilized by a simple constant current controller between the Wehnelt electrode and the filament as shown in Fig.8. The electron beam was chopped by another pair of coils energized by a 500 Hz square wave modulation signal for the lock-in measurement. The chopped beam was permanently monitored by an oscilloscope.

Radiation was detected by a dipole antenna 4 cm long placed at the probe port 1 in Fig.5. The antenna signal was fed, through a stub tuner for impedance matching, to a receiver, Singer model NF-105. The video output signal from the receiver was fed to a lock-in amplifier with a reference signal from the beam modulator and the resultant signal was recorded by an X-Y recorder. The lock-in amplifier was gated by the square wave from the beam modulator. Therefore, the received signal was amplified only while the beam was present. Thus the background was reduced to a minimum. The amplified signal was applied to the Y-input of the recorder, while a signal proportional to the magnetizing current of the uniform field B_1 was applied to the X-input. The radiation spectrum --- radiation intensity versus magnetic field intensity --- was recorded by slowly varying the magnetic field B_1 . The injected electron beam current was also determined by the same lock-in system.

The electron density and temperature of the diffused

plasma in the interaction chamber were measured by a Langmuir probe. The electron density was also determined from the upper hybrid resonance frequency obtained by measuring the spontaneous emission spectrum of the plasma as described in the next section. The values obtained by the two methods agreed within experimental error. The ion saturation current of the Langmuir probe was always monitored for a constant experimental condition.

§4 EXPERIMENTAL RESULTS

Radiation was sought for a wide range of plasma parameters by fixing the receiving frequency ω and varying the strength of the uniform magnetic field B_1 and the plasma source conditions; microwave power and axial position of the cylindrical cavity. Typical examples of the received signal for various densities of the source plasma are shown in Fig.9. The abscissa is the intensity of uniform magnetic field B_1 represented by the ratio ω_{ce}/ω , ω being the fixed receiving frequency, ω_{ce} the electron cyclotron frequency proportional to B_1 . The common experimental conditions were, beam energy $E_b = 20$ keV, beam current $I_b = 0.5$ mA and the fixed receiving frequency $\omega/2\pi = 1.0$ GHz. The signals were detected by a 4 cm dipole antenna located at 10 mm from the center of beam and plasma column. The antenna was immersed in plasma and the dipole was directed parallel to the magnetic field. In the case of Fig.9(a), the plasma source was off and there was only the electron beam injected. Figs. 9(b) through (f) show signals with the plasma source operating. The plasma density was increased in the order from (b) towards (f).

In these figures, the upper traces are direct outputs of the receiver and the lower traces are outputs of the lock-in amplifier. Therefore, the upper traces include spontaneous radiations from the plasma column without beam injection. The receiver supplies the rectified signal of the received RF-signal. Accordingly, its output is

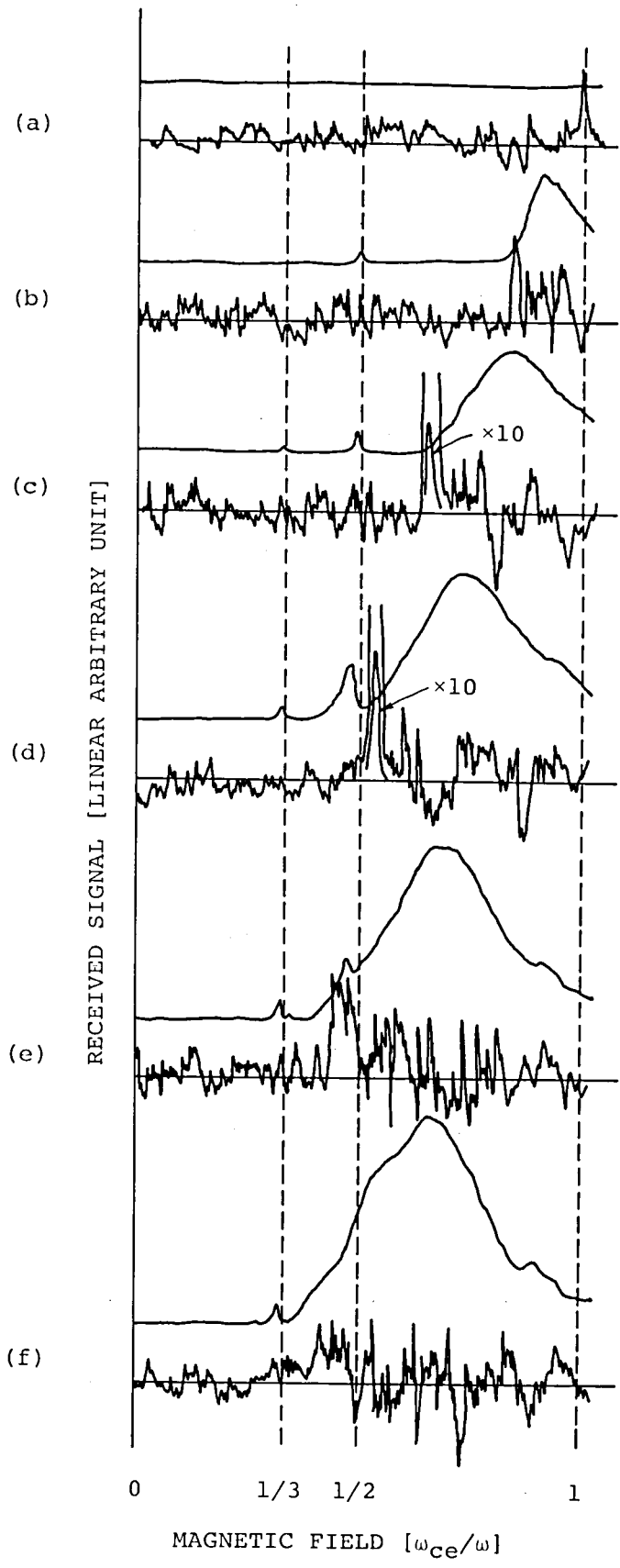


Fig.9. Detected radiation spectra.
 Upper traces; spontaneous radiations from background plasma (output signal of the receiver).
 Lower traces; radiation induced by electron beam (output signal of the lock-in amplifier).
 In (a) the plasma source is off and only the electron beam is present.
 In (b)-(f) the source is operated. Plasma density increases in the order from (b) towards (f).
 Conditions; $p = 5 \times 10^{-5}$ torr Ar, $\beta = 0.272$ (20 keV electron), beam current $I_b = 0.5$ mA, receiving frequency = 1.0 GHz

non-negative and shows smooth variations with increased B_1 or ω_{ce}/ω . On the other hand, the lock-in amplifier yields a positive or negative output according as the receiver output increases or decreases by injection of the electron beam. Therefore, its output shows a rugged behavior when the field intensity is changed. The lower trace of the figure(a) shows the noise level of the receiving system. The small peak at the fundamental cyclotron resonance field may have been a spontaneous emission from the plasma produced by the electron beam injection and disappeared when the beam was off or the neutral gas pressure was reduced. As shown in the upper traces of (b) - (f), some peaks were observed in the direct output of the receiver at field intensities corresponding to cyclotron harmonic resonances, where $\omega/\omega_{ce} = 1/2, 1/3, \dots$. These peaks are of spontaneous emission from the background plasma and were insensitive to the presence of the electron beam. They are believed to be emission due to cyclotron harmonic waves of Bernstein mode in the background plasma with a fairly high electron temperature. The Bernstein wave of extraordinary mode is resonant at each harmonic of the electron cyclotron frequency and the cutoff of the fundamental occurs at the upper hybrid resonance frequency and there are narrow pass-bands just above all higher harmonics of the electron cyclotron frequency¹⁵⁾. The left-hand edge of the large broad peak of the upper trace corresponds to the upper hybrid resonance. Therefore, it forms the upper limit of the pass band in frequency for the Bernstein wave of the fundamental mode.

The position of the upper hybrid resonance was confirmed by measuring the plasma density with a Langmuir probe.

The radiation spectra induced by the electron beam which appeared at the lock-in amplifier output are shown in the lower traces of Fig.9. A sharp peak of radiation was observed just at the magnetic field intensity where the upper hybrid resonance frequency ω_{uh} coincides with the fixed receiving frequency ω . As the plasma density was raised, the radiation peak moved toward a lower field strength B_1 and the amplitude of the peak increased, until the upper hybrid resonance frequency reached the second cyclotron harmonic $2\omega_{ce}$. Fig.10 is a C.M.A. diagram which shows the relation between the magnetic field intensity and the plasma density, both of them being determined when the sharp peak of radiation is appearing in the lower trace of Fig.9. The abscissa is the ion saturation current of the Langmuir probe divided by the square root of the electron temperature determined by the same probe, that is, the abscissa is proportional to the plasma density, while the ordinate is the square of magnetic field B_1^2 . Therefore, the points that the upper hybrid resonance frequency $\omega_{uh} = \sqrt{\omega_{ce}^2 + \omega_{pe}^2}$ becomes equal to the fixed receiving frequency are located on a straight line with a negative incline. The broken horizontal lines indicate that the fixed receiving frequency is equal to the electron cyclotron frequency (upper) or its second harmonic frequency (lower). When the density was so high that the upper hybrid resonance was above the second harmonic of the cyclotron frequency, the radiation

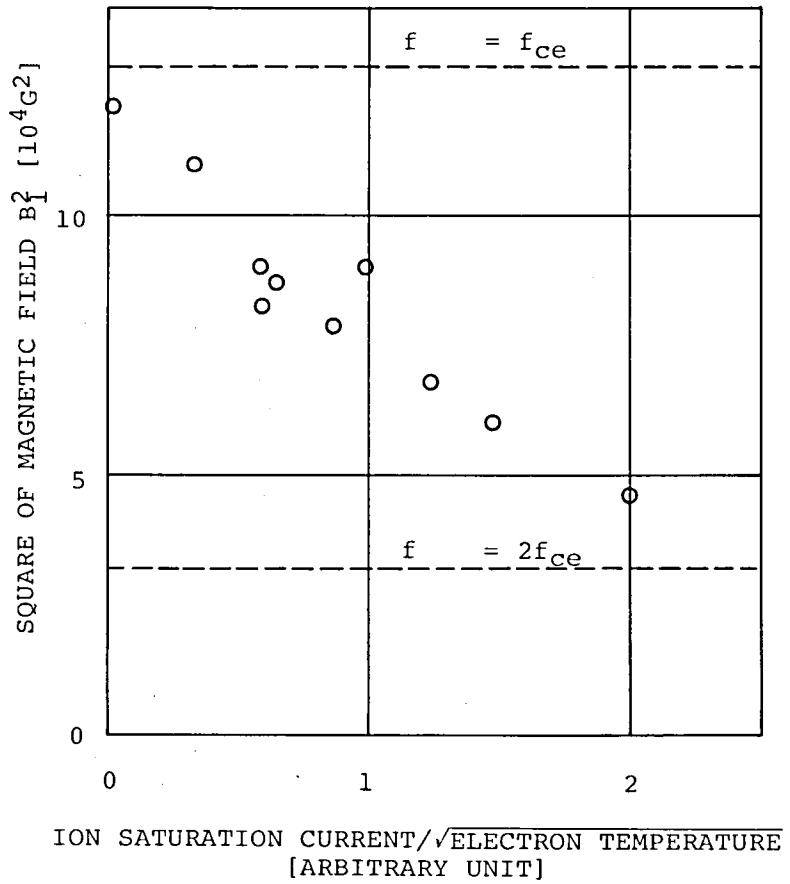


Fig.10. Observed radiation conditions plotted on a C.M.A. diagram. Conditions; the same as Fig.9.

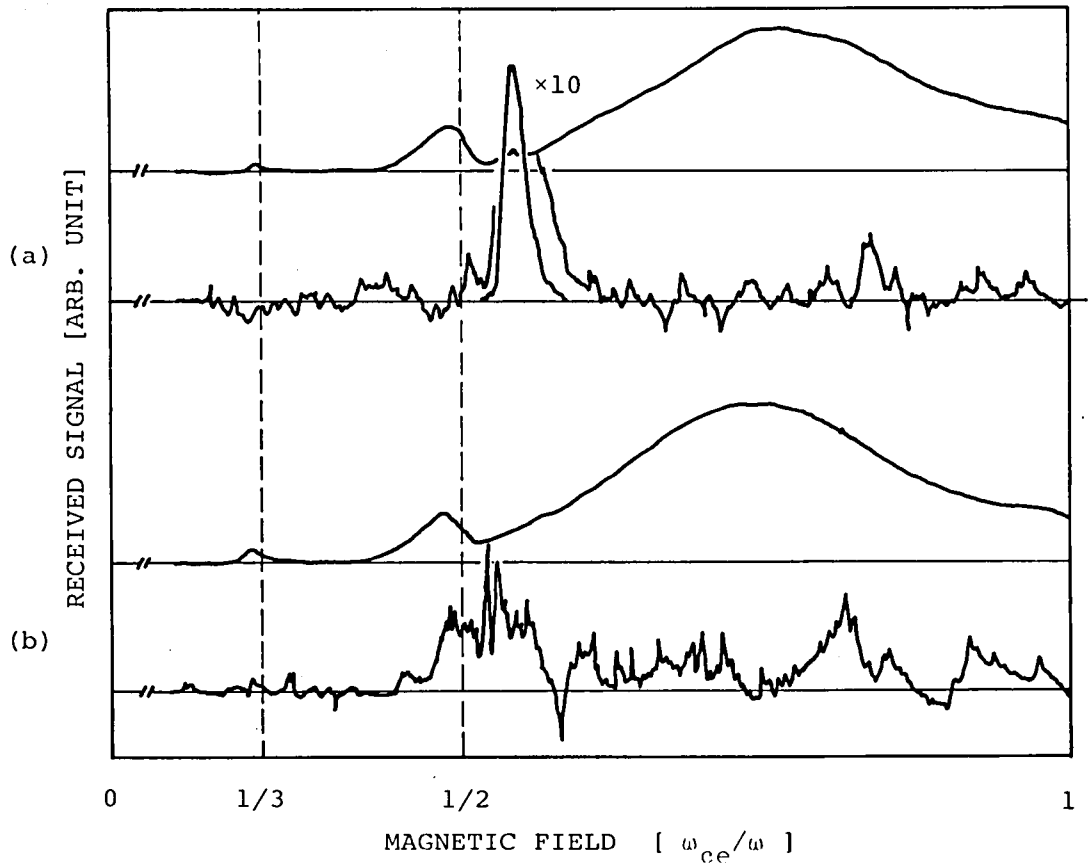


Fig.11. Detected radiation spectra for two plasma densities close the condition that the upper hybrid resonance frequency coincides with the second harmonic of the electron cyclotron frequency.

decreased very sharply as shown in Fig.11, where the plasma density in (b) is slightly higher than in (a).

Frequency spectra of the radiation induced by the electron beam for $B_1 = 220$ G, $n_e = 6 \times 10^9 \text{ cm}^{-3}$, $E_b = 20$ keV and $I_b = 0.25, 1.0$ and 2.0 mA are shown in Fig.12. In this measurement, the stub tuner was removed to avoid any sharp change in sensitivity caused by impedance matching.

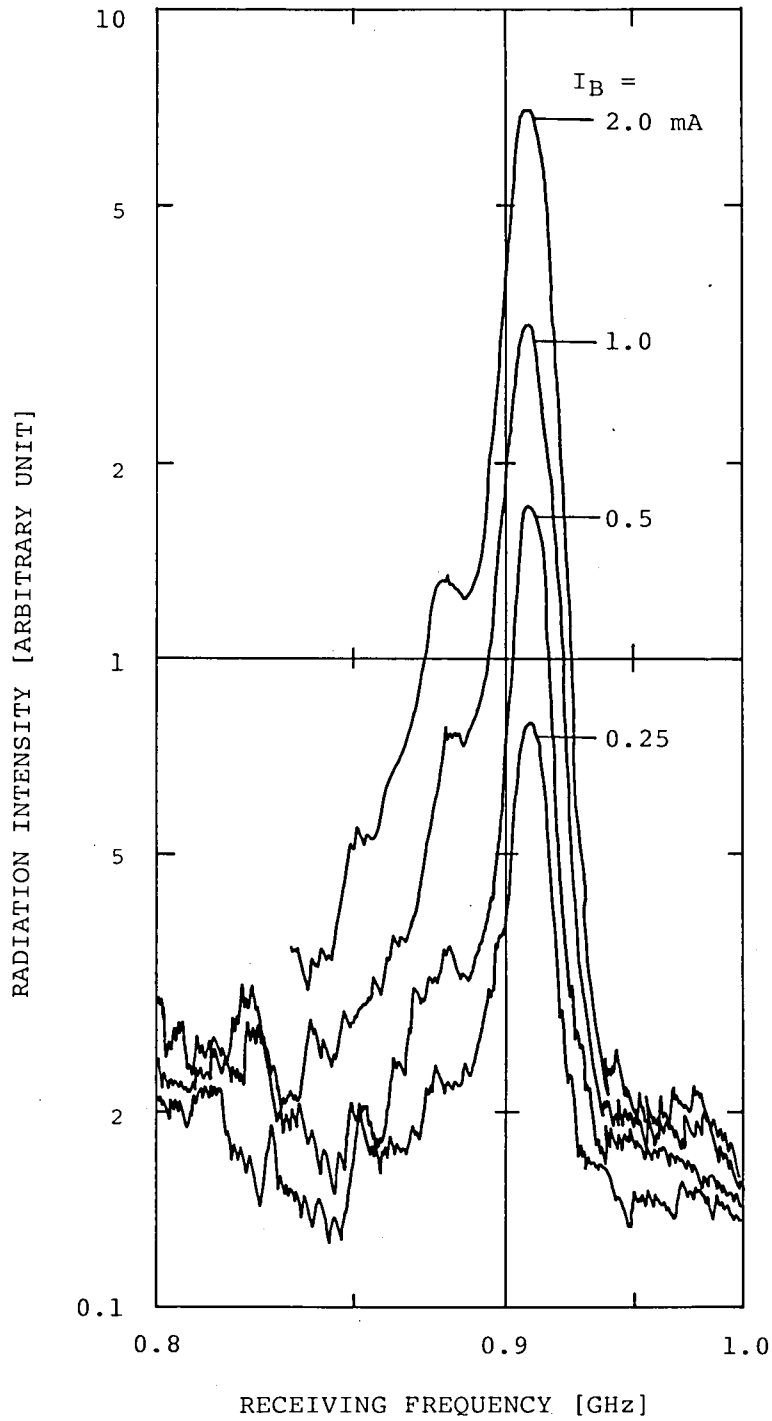


Fig.12. Frequency spectra of the detected signals and its dependence upon beam current. Conditions; $p = 5 \times 10^{-5}$ torr Ar, $B_1 = 220$ G, $n_e = 6 \times 10^9 \text{ cm}^{-3}$, $\beta = 0.272$ (20 keV electron).

A logarithmic converter was used in order to obtain a semi-logarithmic plot by the X-Y recorder. It was observed that the radiation intensity increased in proportion to the beam current without any appreciable change in the spectral shape.

In order to examine the polarization of the radiated wave, the direction of the dipole antenna was rotated. The signal became the most intense when the direction of the dipole was parallel to the magnetic axis and it disappeared when perpendicular to the axis. The dipole antenna must have been carefully adjusted so that its arms were located at the same distance from the center of electron beam. Otherwise, the signal persisted even for the perpendicular direction. It is thought that this occurs because the antenna is sensitive to a radial electric field due to the single pole effect resulting from the wrong positioning of the dipole arms. From the above mentioned observation, it can be concluded that the electric field is strong in the axial and radial directions and weak in the azimuthal direction.

In identifying the Cerenkov radiation, it is important to distinguish the detected radiation from collective phenomena of the other modes. Those collective oscillation are strongly dependent upon the intensity and energy of injected beam. It is for this reason that the relation between the radiation intensity and the beam current was examined for various beam energies. The results are shown in Fig.13. The ordinate is the

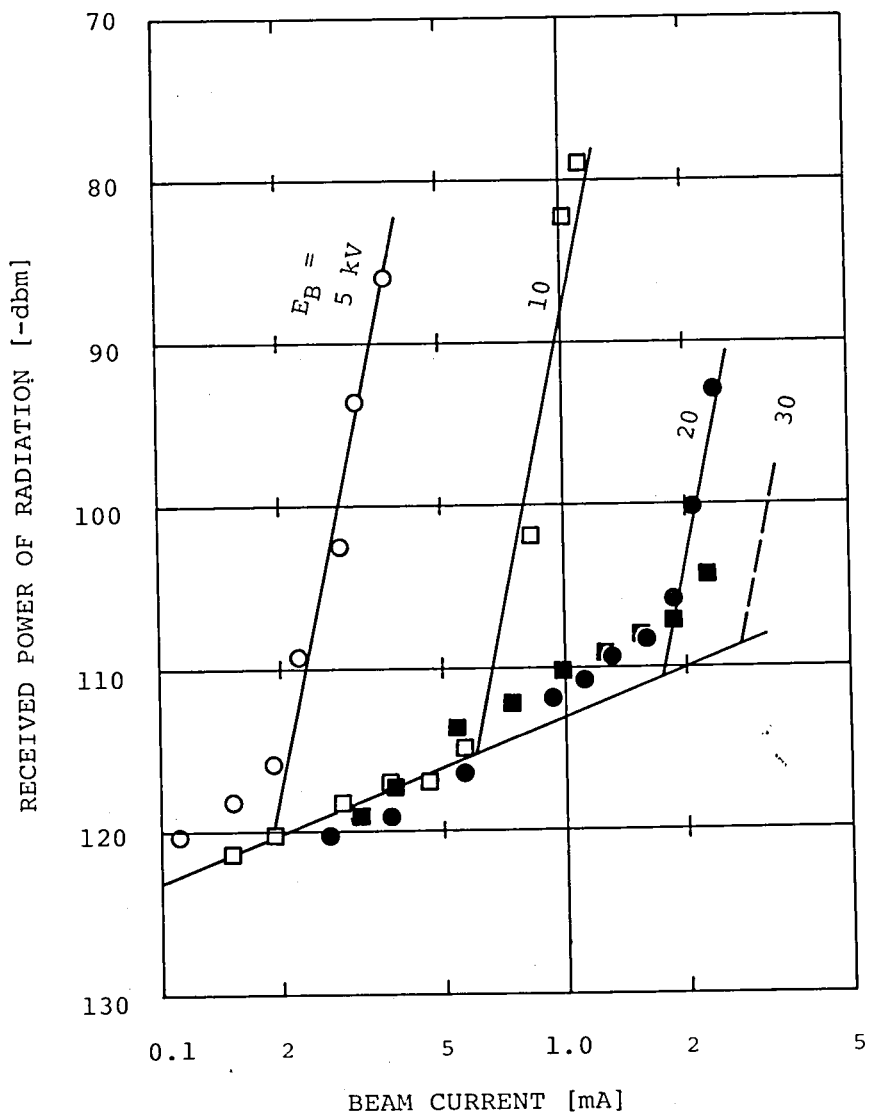


Fig.13. Absolute value of the detected signal and its dependence upon beam energy and beam current. Conditions; $p = 5 \times 10^{-5}$ torr Ar, $B_1 = 200$ G and $n_e = 8.5 \times 10^9 \text{ cm}^{-3}$.

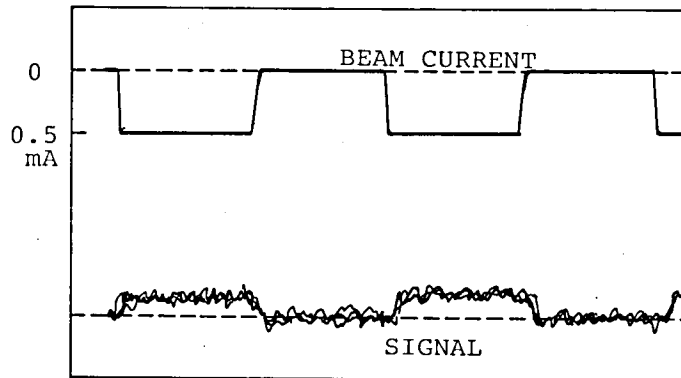
absolute value of radiation intensity obtained by converting the lock-in amplifier output into the power level at the input terminal of the receiver. The overall sensitivity of the receiving system including the lock-in amplifier, converted into the input terminal level, was calibrated for a sinusoidal wave modulated by a square wave of 500 Hz as same as employed in the radiation measurement.

As shown in Fig.13, the radiation intensity increased in proportion to the beam current below a certain critical current. Above the critical current, the intensity increased much more rapidly. In the super-critical region of the beam current, large signal bursts with random intervals were observed at the same time on an oscilloscope connected to the video output of the receiver.

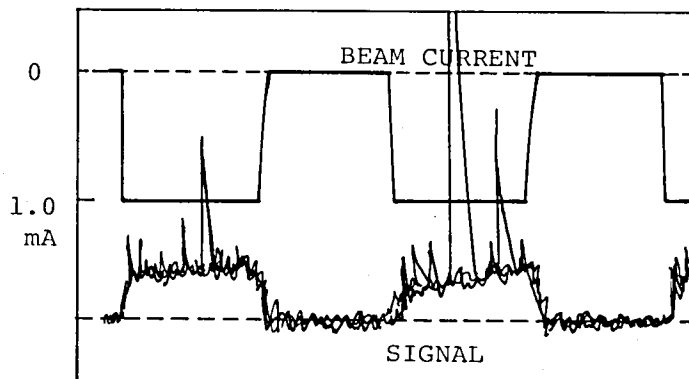
Fig.14(a) shows the sub-critical wave form of the video output, while (b) presents the super-critical rugged wave forms. The rapid increase in radiation intensity was always accompanied by such bursts. The critical beam current depends upon the beam energy; the former is a linear function of the latter in both logarithmic scales as shown in Fig. 15. It has been found from this figure that the critical beam current is proportional to $E_b^{3/2}$, E_b being the beam energy.

In the present study, the radiation belonging to the left branch of Fig.3 with a frequency below the plasma frequency ω_{pe} could not be detected. Possibility of detecting the Cerenkov radiation in this frequency region is left to

future trials with a much higher sensitivity.



(a)



(b)

Fig.14. Wave forms of the video output of the receiver and its dependence upon the beam current. (a) $I_b < I_{critical}$
(b) $I_b > I_{critical}$.

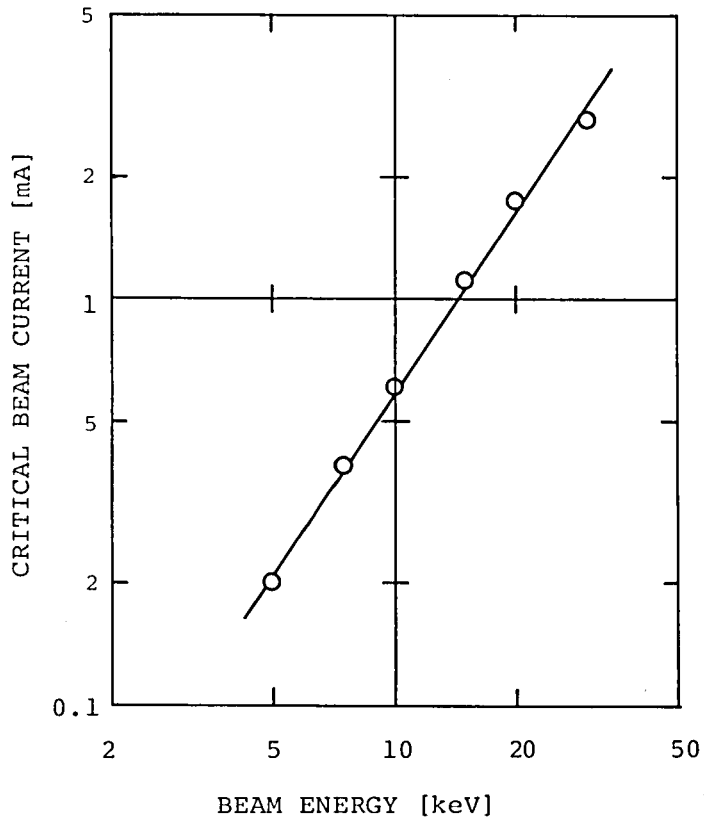


Fig.15. Critical current as a function of beam energy.
 Conditions; the same as Fig.13. The straight line denotes the
 relation; $I_{\text{critical}} \propto E_b^{3/2}$.

§5 COMPARISON OF EXPERIMENTAL RESULTS WITH THEORY

From the stand point that the detected radiation is due to the Cerenkov emission of the extraordinary mode, many of the experimental results are consistent with the theory described in Section 2.

As shown in Fig.9, the radiation appears sharply at the upper hybrid resonance frequency. An evidence can also be seen from the radiation condition shown in the C.M.A. diagram of Fig.10. In this figure, the abscissa is proportional to the plasma density and therefore, to the square of plasma frequency, while the ordinate B_1^2 is proportional to the square of the cyclotron frequency.

In experiments with a fixed receiving frequency ω , the abscissa stands for $(\omega_p/\omega)^2$ and the ordinate for $(\omega_c/\omega)^2$. The upper hybrid resonance frequency $\omega_{uh} = \sqrt{\omega_{ce}^2 + \omega_{pe}^2}$ is represented by a descending straight line on this type of C.M.A. diagram. The experimental points shown in Fig.10 are in good agreement with this theoretical prediction. The divergence of radiation intensity in the theory at the upper hybrid resonance arises from the cold plasma approximation. Taking account of the thermal motion of the plasma electrons, the radiation intensity becomes bounded by Landau damping. Typically in this experiment, the thermal velocity of the plasma electrons v_t was about 2×10^8 cm sec⁻¹, i.e. $c/v_t \approx 150$. The cold plasma approximation, therefore, may fail in the frequency region where the refractive index exceeds 50.

Assuming that the radiation intensity is restricted to the value corresponding to the frequency where the refractive index is equal to 50, we can theoretically estimate the expected absolute value of the radiation intensity and the half-width of the peak of the radiation spectrum from the integrand of equation (20) or (21).

The theoretical half-width is calculated to be 0.1 per cent for $\omega_{pe}/\omega_{ce} = 0.68$, $E_b = 20$ keV, while the observed value is seen from Fig.12 to be 2 per cent.

The broadening of the peak observed in the experiment is thought to be caused by the temporal and spatial fluctuation of the magnetic field B_1 and also by the plasma density fluctuation caused by either the microwave power or the magnetic field B_0 for ECRH, although these were both stabilized to within 1 per cent. The band-width of the receiver is 1 MHz and so is not responsible for the broadening. A narrower resonance can be obtained by reducing fluctuations of the magnetic fields.

As for the absolute value of the radiated power, a single 20 keV electron is theoretically expected to radiate 2×10^{-27} J MHz⁻¹ cm⁻¹ for $n_e = 8.5 \times 10^9$ cm⁻³ and $B_1 = 200$ G. The electron flux is 3×10^{15} sec⁻¹ for a beam current of 0.5 mA. For incoherent radiation, the total radiation power is estimated to be 6×10^{-12} W MHz⁻¹ cm⁻¹ i.e. -82 dbm MHz⁻¹ cm⁻¹. The level of the detected radiation at the input terminal of the receiver is -116 dbm as shown in Fig.13. This difference can partly be attributed to the broadening of resonance peak. Since the theoretically expected

half-width of 0.1 per cent was broadened to 2 per cent (20 MHz) due to the fluctuations in the experimental conditions, this broadening accounts for a loss of -13 db.

The sensitivity of the dipole antenna immersed in plasma column is uncertain. It is, however, certain that noticeable loss was added in the antenna system.

The experimental results concerning the polarization of radiated wave, i.e. that the electric field is strong in the axial and radial directions and weak in the azimuthal direction, coincides with the theoretical behavior of the field components above the plasma frequency as shown in Fig.3.

The phenomenon that radiation disappears at frequencies higher than the second harmonic of the electron cyclotron frequency cannot be explained within the cold plasma theory. This is qualitatively explained as follows: Under the condition of this experiment, intense radiation is expected only in the neighbourhood of the upper hybrid resonance frequency, and then the wave vector of the radiation is nearly perpendicular to the magnetic axis. A theory which includes the thermal motion of plasma electrons for a quasi-perpendicular wave, called the Bernstein mode, has been studied by many researchers; e.g. Crawford et al¹⁵⁾. According to their numerical calculations of the dispersion relation of the Bernstein modes, the group velocity $d\omega/dk_p$ changes its sign when the plasma density is increased and the upper hybrid resonance frequency exceeds the harmonics of the electron cyclotron frequency. Therefore, the Cerenkov radiation may become nonradiative at the harmonic frequency by the

inversion of the direction of energy flow.

The relation between the radiation intensity and the beam current shown in Fig.13 can be explained in connection with the coherence of the emission. The radiation intensity increases in proportion to the beam current until the current exceeds a critical value. This means that there is no correlation among the beam particles and the radiation is incoherent below the critical point. The rapid increase of the radiation above the critical current is believed to arise from the tendency of the emission to become coherent. The wave length of the radiated wave along the beam axis is about 6 cm for $E_p = 10$ keV and frequency = 1 GHz, so that there are 6×10^6 beam electrons per wave length for a beam current of 1 mA. If the emission is perfectly coherent, the radiation intensity can increase to 6×10^6 times the simple sum of the individual radiations. The coherence of radiation and the dependence of the critical current upon beam energy shown in Fig.15 are discussed in the next section in connection with beam-plasma interaction.

§6 DISCUSSION

There may remain a doubt that the RF-radiation observed in this experiment may have some origin other than the Cerenkov effect which leads to the same behavior of radiation.

One possibility is that the beam electrons ionize neutral gas and raise the plasma density and so increase the spontaneous radiation. The mean free path of ionization by collision for 20 keV electrons in argon of gas pressure 5×10^{-5} torr is 8×10^4 cm¹⁴). Therefore, an electron beam of 0.5 mA produces 4×10^{12} pairs of ions and electrons per second in the whole interaction chamber. As it is thought that the particle confinement time is less than 10 μ sec, the number of electrons produced by this process and staying in the chamber is estimated to be less than 4×10^7 . In order to determine experimentally the increase of plasma density due to beam injection, the ion saturation current of the Langmuir probe was measured by the same lock-in system as used in the measurement of radiation spectrum. Its sensitivity is sufficient to detect a density fluctuation of 0.1 per cent. No appreciable increase, however, was detected. Further, it was noticed that the large broad peak in the upper trace of Fig.9 was shifted to the left without any appreciable increase in amplitude, when the plasma density was raised. Therefore, if a small increase in plasma density due to beam injection be the origin of the detected peak in the lower trace of Fig.9, it should have an appearance like the derivative of the broad peak in the

corresponding upper trace; a negative part should appear at the output of the lock-in amplifier in the frequency region of the right side tail of the broad peak in the upper trace. In fact, no such anomalous negative part has ever been exhibited in this frequency region. Thus it may be concluded that such a secondary effect of the injected electron beam is not the origin of the detected radiation.

Next, we examine the relation of the observed signal to the beam-plasma interaction. The Cerenkov radiation is an elementary phenomenon induced by a test particle. In order to identify this process experimentally, it is desirable to use such a weak beam that there is not more than one particle within a Debye sphere of the background plasma. However, this criterion is practically too stringent because detecting the weak radiation due to a single test particle does not seem to be possible. In a typical condition of this experiment, there are 10^3 beam electrons within a Debye sphere. Thus, we must consider the possibility that a beam-plasma interaction causes the same behavior of radiation as detected signal. As previously mentioned in Section 2, the beam-plasma interaction is essentially due to a modulation of the beam density by the propagating wave. It has a growth rate determined by the dispersion relation commonly used in analyses of a beam-plasma system. An emission occurring due to beam-plasma instability is initiated by a thermal noise existing in the background plasma and amplified along the plasma column with the growth rate. In a beam-plasma interaction for such a weak beam

as in this experiment, instability occurs at the crossing point of uncoupled plasma- and beam-dispersion in the ω - k diagram. The strength of the coupling depends upon the beam plasma frequency ω_{pb} . According to the linear theory, the growth rate is proportional to the beam plasma frequency, that is, to the square root of beam current. The observed linear dependence of the radiation power upon beam current is not explained by the beam-plasma interaction, at least within the frame work of linear theory. In general, all the nonlinear effects introduced by saturation of the wave amplitude diminish the growth rate of instabilities caused by the beam-plasma interactions. Consequently, the observed rapid increase of the radiation power above the critical current as shown in Fig.13 cannot be explained in connection with the beam-plasma interaction. In addition, if the interaction be predominant, an increase of beam current should stretch the frequency region for the coupling of plasma waves with beam waves. In such a situation, the spectrum of the observed wave is expected to become wider as well as stronger than it is. As shown in Fig.12, no appreciable change in the spectral shape was actually observed by changing the beam current. Thus it may be concluded that the radiation is due to an elementary process induced by test particles.

Lastly, we consider the transition from the incoherent emission toward the coherent. It is very probable that this transition is brought about by the modulation of the beam particles through a beam-plasma interaction. The theory of a tenuous beam streaming in a magnetoplasma

has been discussed by Briggs¹⁴⁾. According to his theory, transverse reactive-medium amplifications occur just below the lower- and upper-hybrid resonance frequencies. He discussed the stability criteria in connection with a backward-wave oscillator tube. The minimum starting length for oscillation of a backward-wave tube equivalent to the beam-plasma system is given by

$$L_s = Av_0/(\omega_{pb}b)^{2/3}, \quad (24)$$

where b is the beam radius and A is determined by the background plasma parameters. For a given L_s , the minimum beam current for oscillation becomes proportional to $E_b^{3/2}$. This relation agrees with the experimental results shown in Fig.15, which indicates the beautiful relation $I_{\text{critical}} \propto E_b^{3/2}$. The starting length is calculated to be 25 cm for the typical parameters of this experiment; $n_e = 8 \times 10^9 \text{ cm}^{-3}$, $B_1 = 200 \text{ G}$, plasma diameter = 50 mm, $E_b = 20 \text{ keV}$, $I_b = 0.5 \text{ mA}$ and $b = 1 \text{ mm}$. Taking account of assumptions and approximations included in Briggs' theory, the calculated value of starting length may be consistent with the experimental configuration of the interaction chamber.

The pulsed nature of the emission appearing at beam current above the critical value, shown in Fig.14(b), can be explained as follows: At a beam current below the critical value, the radiation is incoherent and appears stationarily in proportion to the beam current as shown in Fig.14(a). When the beam current exceeds the critical value, the beam particles are

bunched through the beam-plasma interaction and the radiation becomes coherent. The rapid growth of wave through the interaction is initiated by a thermal noise of the background plasma by chance, and is terminated after passage of the convective wave packet out of the interaction chamber. Therefore, the coherent radiation appears as a train of high pulses with random intervals as shown in Fig.14(b).

§7 CONCLUSIONS

The emission observed in this experiment is due to the Cerenkov radiation of the extraordinary mode:

- (A) The radiation appears sharply at the upper hybrid resonance frequency as shown in Figs.9 and 10.
- (B) The electric field components of the radiated wave are strong in the axial and radial directions and weak in the azimuthal direction.
- (C) The radiation intensity increases in proportion to the beam current so far as the current does not exceed a critical value as shown in Figs.12 and 13.
- (D) Changing the beam current brings about no appreciable change in the spectral shape of the radiation as shown in Fig.12.
- (E) The radiation intensity increases with the density of the background plasma until the upper hybrid resonance frequency exceeds the second harmonic of the electron cyclotron frequency as shown in Fig.9.
- (F) The absolute value of radiation intensity is consistent with the theoretically expected value, taking account of a certain loss in the sensitivity of antenna system immersed in plasma.

Some doubts that the observed radiation may be caused by some origins other than the Cerenkov effect were checked:

- (G) Spontaneous radiation from the additional plasma produced by beam injection is not the origin of the observed radiation, because no plasma density fluctuation synchronous with beam injection was observed and the spectral shape expected for the radiation due to this process is different from the observed.
- (H) Beam-plasma interaction is not the direct source of the observed radiation, because the spectral shape is independent of the beam current as shown in Fig.12 and a stationary emission proportional to the beam wave form, as shown in Fig.14(a), is observed.

Transition from the incoherent Cerenkov radiation to the coherent is caused through a thin beam-plasma interaction.

- (I) The radiation intensity increases much more rapidly than proportionally to the beam current when the current exceeds a critical value as shown in Fig.13.
- This rapid increase is caused through the transition.
- (J) The dependence of the critical current upon the beam energy is given by $I_{\text{critical}} \propto E_b^{3/2}$ as shown in Fig.15. This dependence coincides with Briggs' stability criterion of a thin beam-plasma system.
- (K) The experimental condition when the transition occurs is quantitatively consistent with the stability criterion derived by Briggs.
- (L) The pulsed nature of the emission appearing at beam current above the critical value, as shown in Fig.14(b),

is explained by the fact that beam-bunching through the beam-plasma interaction is initiated by a thermal noise in the background plasma.

Others

- (M) The Cerenkov radiation disappears suddenly when the upper hybrid resonance frequency exceeds the second harmonic of the electron cyclotron frequency as shown in Fig.11. This phenomenon is qualitatively explained by taking account of thermal motion of the plasma in connection with dispersion relation of the Bernstein mode.
- (N) The Cerenkov radiation of ordinary mode expected theoretically could not be detected in this experiment. It is difficult to detect the radiation among background noise because the mode is weak in radiation intensity and has no noticeable feature such as the resonant peak in case of the extraordinary mode.

ACKNOWLEDGEMENT

The author would like to thank Professor Hiroshi Nishihara for his support and encouragement of this research and for his constructive suggestions during the preparation of this manuscript; J. Hamano for his co-operation in preliminary experiment; and Y. Shimidzu and N. Ide for the construction of the experimental apparatus.

REFERENCES

- 1) G.Bekefi; Radiation Processes in Plasma, Wiley, New York (1966).
- 2) I.E.Tamm and I.M.Frank; Dokl. Akad. Nauk. SSSR 14, 109 (1937).
- 3) J.V.Jelly; Cerenkov Radiation, Pergamon Press, New York, (1958).
- 4) V.L.Ginzburg; Soviet Physics Uspekhi, 2, 874 (1960).
- 5) A.A.Kolomenski; Dokl. Akad. Nauk. SSSR, 106, 982 (1955).
- 6) V.N.Kurdyumov; Soviet Phys.-Tech. Phys. 10, 1370 (1966).
- 7) V.N.Kurdyumov; Soviet Phys.-Tech. Phys. 11, 441 (1967).
- 8) R.Sasiela and J.P.Freidberg; Radio Science 2, 703 (1967).
- 9) H.Kikuchi; Proc. of the Symposium on Quasi-Optics, 235 Polytechnic Press, Brooklyn (1958).
- 10) B.J.Eastlund; Nucl. Fusion 11, 15 (1971).
- 11) Y.Mizumachi, K.Nishikawa and T.Nishikawa; J. Phys. Soc. Japan 34, 1083 (1973).
- 12) W.P.Allis, S.J.Buchsbaum and A.Bers; Waves in Anisotropic Plasmas, M.I.T. press, Massachusetts (1963).
- 13) T.H.Stix; The Theory of Plasma Waves, McGraw-Hill, New York (1962).
- 14) R.J.Briggs; Electron-Stream Interaction with Plasma, M.I.T. Press, Massachusetts (1966).
- 15) F.W.Crawford and J.A.Tataronis; Stanford Univ. Internal Memo. on Contract(NSF GP-936) Report No. 1295 (1965).
- 16) L.J.Kieffer and G.H.Dunn; Rev. Mod. Phys. 38, 1 (1966).

Appendix A Cerenkov Radiation in an Isotropic Medium

In equation (3), replacing the dielectric tensor $\vec{\vec{K}}$ by a dielectric constant ϵ , we obtain

$$(k^2 - \vec{k}\vec{k} \cdot - k_0^2 \epsilon) \vec{E} = 2\pi i \mu_0 \omega q \vec{v}_0 \delta(k_z v_0 - \omega), \quad (\text{A-1})$$

where all symbols are the same in the body.

The component of electric field parallel to the charge velocity is given by

$$E_z(\vec{k}, \omega) = -2\pi i \mu_0 \omega q v_0 \delta(k_z v_0 - \omega) \frac{k_z^2 - k_0^2 \epsilon}{k_0^2 (k^2 - k_0^2 \epsilon)}. \quad (\text{A-2})$$

By inverse Fourier transformation, we obtain

$$E_z(\vec{r}, t) = - \frac{i \mu_0 q v_0}{(2\pi)^3} \int_{-\infty}^{\infty} \omega d\omega \int_{-\infty}^{\infty} \int_{-\infty}^{\infty} d^3 \vec{k} e^{i(\vec{k} \cdot \vec{r} - \omega t)} \times \frac{k_z^2 - k_0^2 \epsilon}{k_0^2 (k^2 - k_0^2 \epsilon)} \delta(k_z v_0 - \omega). \quad (\text{A-3})$$

The radiation energy per unit path is given by the frictional force $F = -qE_z$ reacting on the charge;

$$\begin{aligned} \frac{dW}{dz} &= -qE_z(\vec{r} = \vec{v}_0 t) \\ &= - \frac{i \mu_0 q^2}{(2\pi)^3} \int_{-\infty}^{\infty} \omega d\omega \int_{-\infty}^{\infty} \int_{-\infty}^{\infty} d^2 \vec{k}_t \frac{\epsilon - \beta^{-2}}{[k_t^2 - k_0^2 (\epsilon - \beta^{-2})]} \\ &= - \frac{i \mu_0 q^2}{8\pi^2} \int_{-\infty}^{\infty} \omega d\omega \int_0^{\infty} dk^2 \left(1 - \frac{1}{\epsilon \beta^2}\right) \frac{1}{k^2 - (\epsilon - \beta^{-2})}. \quad (\text{A-4}) \end{aligned}$$

where \vec{k}_t is the propagation vector perpendicular to the charge velocity and $\kappa = k_r/k_0$ with $k_r = |\vec{k}_t|$. When $\epsilon < \beta^{-2}$ i.e. $v_0^2 < c^2/\epsilon$, the integral vanishes because the dielectric constant ϵ is unchanged for reversion of propagation direction of light, i.e. ϵ is an even function of ω .

When $\epsilon > \beta^{-2}$, the integral becomes a singular integral, whose principal part vanishes. In order to calculate the singular part, we must determine the integration path in the neighbourhood of the positive pole $\kappa^2 = \epsilon - \beta^{-2}$. We introduce a small conductivity into the Maxwell equations as a dissipation in dielectric polarization;

$$\frac{1}{\mu_0} i\vec{k} \times \vec{B} = -i\omega\epsilon_0\epsilon\vec{E} + \sigma\vec{E} + \vec{j}, \quad (\text{A-5})$$

where $\sigma > 0$ and \vec{j} denotes the current due to the moving charge. Letting the conductivity σ be included in the dielectric constant, an imaginary part is added to ϵ ;

$$\epsilon \rightarrow \epsilon + \frac{i\sigma}{\omega\epsilon_0}. \quad (\text{A-6})$$

The imaginary part is positive for $\omega > 0$ and negative for $\omega < 0$. The integration path for κ^2 , therefore, must be taken as shown in Fig.A. Dividing the ω -integral into two parts for positive ω and negative ω and taking the difference;

$$\int_{-\infty}^{\infty} \omega d\omega f(\omega) = \left(\int_0^{\infty} + \int_{-\infty}^0 \right) \omega d\omega f(\omega) = \int_0^{\infty} \omega d\omega [f(\omega) - f(-\omega)]. \quad (\text{A-7})$$

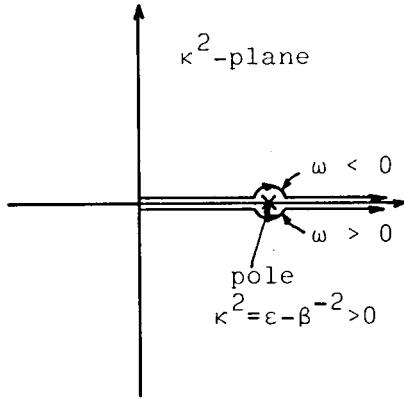


Fig.A. Integration path of equation (A-4) .

Thus the κ^2 -integral is replaced by the residue at the positive pole;

$$\int_0^{\infty} d\kappa^2 \frac{1}{\kappa^2 - (\epsilon - \beta^{-2})} = 2\pi i \text{ for } \omega > 0 \quad (\text{A-8})$$

Therefore, the radiation energy per unit path is given by

$$\frac{dW}{dz} = \frac{\mu_0 q^2}{4\pi} \int_{\epsilon > \beta^{-2}}^{\infty} \omega d\omega \left(1 - \frac{1}{\epsilon \beta^2}\right) \quad (\text{A-9})$$

The integral never diverges because $\beta < 1$ and for all materials

$$\lim_{\omega \rightarrow \infty} \epsilon = 1 \quad (\text{A-10})$$

From the positive pole $\kappa^2 = \epsilon - \beta^{-2}$, the Cerenkov condition

$$\cos^2 \theta = \frac{k_r^2}{k^2} = \frac{c^2}{\epsilon v^2}, \quad n^2 = \epsilon \quad (\text{A-11})$$

is easily derived.

Appendix B Derivation of Dielectric Tensor

of Cold Electron Plasma

We consider that ions and electrons are uniformly distributed in space and a uniform magnetic field \vec{B} is applied. It is assumed that only electrons are perturbed by an electric field \vec{E} .

Equation of motion for electrons is given by

$$m \frac{d\vec{v}}{dt} = q(\vec{E} + \vec{v} \times \vec{B}) - m\vec{v}\nu, \quad (\text{B-1})$$

where m and q are mass and charge of electron, respectively. The last term $-m\vec{v}\nu$ denotes Langevin force due to collisions of electron with ions and/or neutral atoms where ν is the collision frequency. Electric displacement \vec{D} is expressed with dielectric tensor \vec{K} or conductivity tensor $\vec{\sigma}$ as follows;

$$\begin{aligned} \vec{D} &\equiv \epsilon_0 \vec{K} \cdot \vec{E} = \epsilon_0 \vec{E} + \frac{1}{i\omega} \vec{j} \\ &= \left(\epsilon_0 + \frac{\vec{\sigma}}{i\omega} \right) \vec{E} \end{aligned} \quad (\text{B-2})$$

and

$$\vec{j} = ne\vec{v} \quad (\text{B-3})$$

where n is electron number density.

Notice that in equations (B-1) and (B-3), \vec{v} and \vec{E} are perturbed quantities, then we may take account of the average values of \vec{B} and n because their perturbations are infinitesimals of higher order. Assuming that the perturbed quantities vary with plane wave dependence $\exp[i(\vec{k} \cdot \vec{r} - \omega t)]$, equation (B-1) becomes

$$-im(\omega + iv)\vec{v} = q(\vec{E} + \vec{v} \times \vec{B}). \quad (\text{B-4})$$

Taking z-axis along B, the components are written as

$$\begin{aligned} -i(\omega + iv)v_x + \omega_{ce}v_y &= (q/m)E_x \\ -i(\omega + iv)v_y - \omega_{ce}v_x &= (q/m)E_y \\ -i(\omega + iv)v_z &= (q/m)E_z \end{aligned} \quad (\text{B-5})$$

where $\omega_{ce} = \left| \frac{qB}{m} \right|$ is the electron cyclotron frequency. Substituting equation (B-5) into equation (B-2), \vec{K} is expressed as follows;

$$\vec{K} \equiv \begin{pmatrix} \epsilon_{xx} & \epsilon_{xy} & 0 \\ \epsilon_{yx} & \epsilon_{yy} & 0 \\ 0 & 0 & \epsilon_{zz} \end{pmatrix} \quad (\text{B-6})$$

where

$$\begin{aligned} \epsilon_{xx} = \epsilon_{yy} &= 1 - \frac{\omega_{pe}^2(\omega + iv)}{\omega[(\omega + iv)^2 - \omega_{ce}^2]} \\ \epsilon_{xy} = -\epsilon_{yx} &= \frac{i\omega_{pe}^2\omega_{ce}}{\omega[(\omega + iv)^2 - \omega_{ce}^2]} \\ \epsilon_{zz} &= 1 - \frac{\omega_{pe}^2}{\omega(\omega + iv)} \end{aligned} \quad (\text{B-7})$$

where $\omega_{pe} = (nq^2/\epsilon_0 m)^{1/2}$ is the electron plasma frequency. When $\nu \rightarrow 0$, equations (B-6) and (B-7) become equations (4) and (5) in the body.